Stossel, T. P. (1989) *J. Biol. Chem. 264*, 18261-18264.
Truglia, J. A., & Stracher, A. (1981) *Biochem. Biophys. Res. Commun. 100*, 814-822.
Tyler, J. M., Anderson, J. M., & Branton, D. (1980) *J. Cell Biol. 85*, 489-495.
Wallach, D., Davies, P. J. A., & Pastan, I. (1978a) *J. Biol. Chem. 253*, 3328-3335.
Wallach, D., Davies, P. J. A., & Pastan, I. (1978b) *J. Biol. Chem. 253*, 4739-4745.
Wang, K. (1977) *Biochemistry 16*, 1857-1865.
Wang, K., & Singer, S. J. (1977) *Proc. Natl. Acad. Sci. U.S.A. 74*, 2021-2025.
Wang, K., Ash, J. F., & Singer, S. J. (1975) *Proc. Natl. Acad. Sci. U.S.A. 72*, 4483-4486.
Weihing, R. R. (1983) *Biochemistry 22*, 1839-1847.
Weihing, R. R. (1985) *Can. J. Biochem. Cell Biol. 63*, 397-413.
Weihing, R. R. (1988) *Biochemistry 27*, 1865-1869.
Weihing, R. R., & Franklin, J. S. (1983) *Cell Motil. 3*, 535-543.

Solution Structure of the Nogalamycin–DNA Complex†

Xiaolu Zhang and Dinshaw J. Patel*
Department of Biochemistry and Molecular Biophysics, College of Physicians and Surgeons, Columbia University, New York, New York 10032

Received May 21, 1990; Revised Manuscript Received July 10, 1990

ABSTRACT: The nogalamycin–d(A-G-C-A-T-G-C-T) complex (two drugs per duplex) has been generated in aqueous solution and its structure characterized by a combined application of two-dimensional NMR experiments and molecular dynamics calculations. Two equivalents of nogalamycin binds to the self-complementary octanucleotide duplex with retention of 2-fold symmetry in solution. We have assigned the proton resonances of nogalamycin and the d(A1-G2-C3-A4-T5-G6-C7-T8) duplex in the complex and identified the intermolecular proton–proton NOEs that define the alignment of the antitumor agent at its binding site on duplex DNA. The analysis was greatly aided by a large number of intermolecular NOEs involving exchangeable protons on both the nogalamycin and the DNA in the complex. The molecular dynamics calculations were guided by 274 intramolecular nucleic acid distance constraints, 90 intramolecular nogalamycin distance constraints, and 104 intermolecular distance constraints between nogalamycin and the nucleic acid protons in the complex. The aglycon chromophore intercalates at (C-A)·(T-G) steps with the long axis of the aglycon approximately perpendicular to the long axis of the flanking C3·G6 and A4·T5 base pairs. The aglycon selectively stacks over T5 and G6 on the T5-G6-containing strand with the aglycon edge containing OH-4 and OH-6 substituents directed toward the C3-A4-containing strand. The C3·G6 and A4·T5 base pairs are intact but buckled at the intercalation site with a wedge-shaped alignment of C3 and A4 on the C3-A4 strand compared to the parallel alignment of T5 and G6 on the T5-G6 strand in the complex. The nogalose sugar in a chair conformation, the aglycon ring A in a half-chair conformation, and the $COOCH_3$-10 side chain form a continuous domain that is sandwiched within the walls of the minor groove and spans the three base pair (G2-C3-A4)·(T5-G6-C7) segment. The nogalose ring is positioned in the minor groove such that its nonpolar face is directed toward the G6-C7 sugar–phosphate backbone while its polar face containing OCH_3 groups is directed toward the G2-C3 sugar–phosphate backbone in the complex. The intermolecular contacts include a nonpolar patch of aglycon (CH_3-9) and nogalose (CH_3-3′) methyl groups forming van der Waals contacts with the base–sugar residues in the minor groove and intermolecular hydrogen bonds involving the amino groups of G2 and G6 with the ether oxygens OCH_3-3′ and O7, respectively, on the nogalose sugar. The bicyclic amino sugar adopts a chair conformation and is positioned in the major groove. The intermolecular contacts include a hydrophobic patch involving the bridgehead H1″ and CH_3-5″ protons on the bicyclic amino sugar and the CH_3 groups of T5, establishing the contribution of the thymidine to intercalation specificity at (C-A)·(T-G) steps in DNA. A pair of intermolecular hydrogen bonds stabilizes the alignment of the bicyclic amino sugar in the major groove and is formed between the bicyclic amino sugar OH-2″ and OH-4″ protons which are directed toward the N7 and O6 atoms of G6 in the complex. The nogalose and bicyclic amino sugars of nogalamycin move toward each other on complex formation with DNA in order to maximize the intermolecular contacts in both grooves of the duplex. The above details of the solution structure of the nogalamycin–DNA complex provide insights into the intermolecular contacts involving the drug's intercalating, minor groove, and major groove components and explain the sequence specificity of this antitumor agent for intercalation between G·C and A·T pairs at the (G-C-A)·(T-G-C) trinucleotide segment on the d(A-G-C-A-T-G-C-T) duplex.

Nogalamycin (**1**), isolated from *Streptomyces nogalator*, is a member of the anthracycline family of antibiotics, which exhibit significant antitumor and antibacterial activity (Bhuyan & Reusser, 1970; Li et al., 1979). Nogalamycin binds to DNA and selectively inhibits DNA-directed RNA synthesis in vivo (Fok & Waring, 1972; Ennis, 1981).

† This research was funded by NIH CA-46778.

0006-2960/90/0429-9451$02.50/0

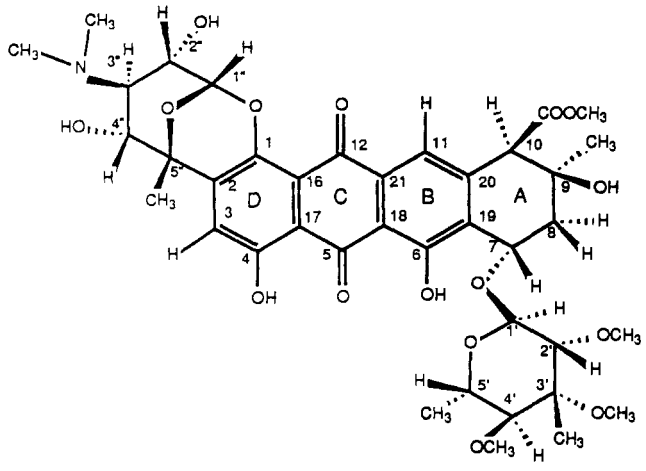

1

Sedimentation and viscosity measurements have established that nogalamycin binds to DNA through intercalation, resulting in stabilization of the double helix (Kersten et al., 1966; Das et al., 1974; Sinha et al., 1977; Gale et al., 1981). The aglycon ring of nogalamycin is substituted at one end of its long axis by a positively charged bicyclic amino sugar fused to the C1 and C2 positions and substituted at the other end by a nogalose sugar attached to the C7 position. The slow association and dissociation kinetics observed for nogalamycin–DNA complexes (Fox & Waring, 1984; Fox et al., 1985) must reflect the local melting of the DNA helix associated with insertion and release of the dumbbell-shaped antitumor agent.

Footprinting studies have established a sequence preference of nogalamycin for (C-A)·(T-G) pyrimidine–purine steps on duplex DNA (Fox & Waring, 1986; White & Phillips, 1989) preferentially in the sequence context (G-C-A)·(T-G-C). The observed pyrimidine–purine sequence preference has permitted formation of the nogalamycin–d(G-C-A-T-G-C) complex (two drugs per duplex) for structural studies in solution (Searle et al., 1988) and the nogalamycin–d(*C-G-TsA-*C-G) complex (two drugs per duplex) for structural studies in the crystalline state (Liaw et al., 1989; Williams et al., 1990).

We report below on structural NMR studies of the nogalamycin–d(A-G-C-A-T-G-C-T) complex (two drugs per duplex) in H_2O and D_2O solution. These studies combine two-dimensional NMR and molecular dynamics computations to define the solution structure of the nogalamycin–d(A-G-C-A-T-G-C-T) complex.

Materials and Methods

Oligonucleotide Synthesis. The d(A-G-C-A-T-G-C-T) octanucleotide was synthesized on a Beckman System 1 plus DNA synthesizer with the solid-phase cyanoethyl phosphoramidite method. The crude 5′-dimethoxytritylated octanucleotide was isolated by treatment of the support with concentrated aqueous ammonia for 45 h at room temperature. The octanucleotide was then purified by reverse-phase HPLC in two stages and desalted on a Sephadex G-25 column. The oligomer was finally converted to the sodium form on a Dowex 50X8 cation exchange column.

Nogalamycin–Oligonucleotide Complex. Nogalamycin was provided by the Upjohn Co. About 3 equiv of solid nogalamycin was directly added to 0.45 mL of the d(A-G-C-A-T-G-C-T) duplex in aqueous buffer solution (0.1 M NaCl, 10 mM phosphate, 0.1 mM EDTA). The mixture was diluted to 5 mL with water and shaken in a cold room for 24 h. The solution was then lyophilized and redissolved in 0.45 mL of H_2O. The excess nogalamycin, which was insoluble at neutral pH, was removed by centrifugation.

The nogalamycin–d(A-G-C-A-T-G-C-T) complex (concentration ~4 mM) was adjusted to an uncorrected glass electrode pH reading of 6.7 with dilute NaOH or HCl. For experiments in H_2O, the complex was lyophilized and then redissolved in 0.45 mL of 90% H_2O/10% D_2O. For experiments in D_2O, the complex was first lyophilized, redissolved in 99.8% D_2O, and relyophilized. This procedure was repeated three times with the complex finally dissolved in 0.45 mL of 99.96% D_2O under nitrogen gas.

NMR Experiments. All NMR spectra were recorded on Bruker AM 500 or Varian XL400 spectrometers. Quadrature detection was used in both dimensions with the carrier frequency placed on the H_2O resonance for all experiments. All data sets were transferred to a VAX 11-780 or a micro VAX II computer and processed with the FORTRAN program FTNMR provided by Dr. Dennis Hare (Hare Research). The FIDs for the initial t_1 value in each 2D data set were multiplied by 0.5 in order to eliminate t_1 ridge artifacts.

Two-dimensional data sets on the complex in D_2O buffer were recorded on a Bruker AM 500 spectrometer. The sample temperature was 30 ± 0.5 °C. The spectral width was 5000 Hz (10 ppm). All spectra were acquired without irradiation of the residual water signal, which was small due to extensive lyophilization from D_2O of the sample. The COSY spectrum was collected with 1024 complex points in t_2, 310 complex free induction decays (FIDs) in t_1, 96 transients for each FID, and a repetition delay of 1.3 s. Both time domain data sets were multiplied by a 0° phase-shifted sine bell window function. A set of NOESY spectra with mixing times of 50, 75, and 100 ms were recorded with 1024 complex points in t_2, 400 complex FIDs in t_1, 64 transients for each FID, and a repetition delay of 1.3 s. Both time domain data sets were multiplied by a 70° phase-shifted sine bell window function.

Two NOESY data sets with mixing time of 150 and 200 ms were recorded on a Varian XL400 spectrometer on the complex in H_2O buffer solution. The sample temperature was 25 ± 0.5 °C. The spectral width was 8000 Hz (20 ppm). The NOESY spectra were recorded without irradiation of water signal. The water signal was suppressed by application of a combined homospoil pulse and a water suppression pulse sequence as the detection pulse. The pulse sequence used in this experiment is

$$[t_0\text{–}90°\text{–}t_1\text{–}90°\text{–}t_m\text{–}(90°_x\text{–}\Delta\text{–}90°_{-x})\text{–}t_2\text{–}]_n$$

The relaxation time t_0 was 1.3 s. The delay Δ was set to 80 μs to optimize the excitation in imino, amino, and aromatic proton regions of the spectrum. A 10-ms homospoil pulse was used during mixing time t_m in order to suppress the water signal. The spectra were collected with 1024 complex points in t_2, 400 complex FIDs in t_1, and 32 transients for each FID. Both time domain data sets were multiplied by a 70° phase-shifted sine bell window function.

Interproton Distance Constraints. The cross peaks in a NOESY spectrum represent dipole–dipole couplings between nuclei that are within 5 Å of each other. The intensities of these NOE cross peaks provide information about the internuclear distance on the basis of the relationship

$$\text{NOE} \propto f(\tau_c)(1/r^6) \quad (1)$$

where $f(\tau_c)$ is a function of the correlation time τ_c and represents the influence of the motion of the molecule on the observed NOE. The correlation time τ_c can be defined as the average time for a molecule to rotate by 1 rad for reorientational motion. The correlation time of a molecule in solution will be affected by the molecular size and the temperature and

viscosity of the solution. In principle, given a known distance r_{kl}, the unknown distance r_{ij} can be directly calculated from

$$r_{ij} = r_{kl}(\mathrm{NOE}_{kl}/\mathrm{NOE}_{ij})^{1/6} \quad (2)$$

where NOE_{kl} and NOE_{ij} are the NOEs between atoms k and l and atoms i and j, respectively. However, the validity of eqs 1 and 2 is limited. First, eq 1 is valid only for two-spin relaxation or direct magnetization transfer while in practice NOE cross peaks result from multispin relaxation. The assumption that NOEs result only from direct magnetization transfer will be valid only for NOEs measured from NOESY spectra recorded with extremely short mixing times. Unfortunately, signal-to-noise ratios are usually quite poor at short mixing times. Studies have shown that the effect of indirect magnetization transfer can cause significant errors for estimation of distances from NOESY spectra. Borgias and James (1988) have quantitatively estimated the errors caused by ignoring indirect magnetization transfer and indicate that the errors for a calculated distance of 3 Å range from ±0.50 Å in a 50-ms NOESY spectrum to ±0.80 Å in a 250-ms NOESY spectrum.

Second, the $f(\tau_c)$ term in eq 1 can be canceled in eq 2 only under the assumption that the molecule tumbles as a rigid isotropic unit where all interproton vectors have the same effective correlation times. In most cases, macromolecules are not rigid bodies, and internal motions in the molecule cause different effective correlation times for different interproton vectors. The errors caused by use of the second assumption have been estimated to be ~10% in calculated distances (Lane, 1988; Borgias & James, 1988).

The volume integrals of individual NOE cross peaks in the nogalamycin–d(A-G-C-A-T-G-C-T) complex were measured from NOESY contour plots recorded with a mixing time of 50 ms in D_2O and 150 ms in H_2O solution. Since eq 2 is only valid when the effective correlation times of the i–j and k–l interproton vectors are the same, the reference distances in the calculation of the unknown interproton distances have to be chosen appropriately. In the case of oligonucleotides, the fixed distances corresponding to sugar H2′–H2″ and cytidine H5–H6 can be used as the reference distances. NMR studies of DNA oligomers have shown that the effective correlation times of sugar H2′–H2″ vectors are significantly shorter than those of the cytidine H5–H6 vectors (Clore & Gronenborn, 1984; Gronenborn & Clore, 1985; Gronenborn et al., 1984). Considering that the contribution from internal motion to the effective correlation times of the sugar–sugar and sugar–base distances will mainly be dominated by motion within the sugar units, while that of the base–base will mainly be dominated by motion about the glycosidic bond, it has been suggested that all unknown distances involving sugar–sugar and sugar–base vectors, except sugar H1′–base vectors, should be calculated with the r[H2′–H2″] as a reference and all those involving base–base and sugar H1′–base vectors should be calculated with r[C(H5)–C(H6)] as a reference. In this work, we used an r[H2′–H2″] distance of 1.8 Å as a reference distance in the calculation of the unknown interproton distances involving sugar–sugar and sugar–base vectors in DNA, except the sugar H1′–base vector. The r[C(H5)–C(H6)] distance of 2.45 Å was used as a reference distance in the calculation of the unknown interproton distances involving base–base and sugar H1′–base vectors in DNA. The geminal r[H8–H8] distance of 1.8 Å on the nogalamycin aglycon ring A was used as a reference distance in the calculation of all unknown interproton distances for nogalamycin in the complex.

It has been recently suggested that r[C(H5)–C(H6)] should be used as the reference for estimating proton–proton distances for all pairs in DNA oligomer duplexes (Nerdal et al., 1988). However, it should be noted that on the basis of r[C(H5)–C(H6)] as the reference distance, we calculate r[H2′–H2″] to be 2.14 Å (averaged), which is 0.34 Å longer than the actual fixed distance of 1.8 Å.

The intermolecular proton–proton distances defined by lower and upper bounds for the nogalamycin–d(A-G-C-A-T-G-C-T) complex listed in Tables V and VI were estimated with r[C(H5)–C(H6)] as the reference distance.

The approach we used for calculation of distances is based on the assumptions discussed above and leads to errors in the calculated distances. Thus, each input distance constraint is defined by an upper and lower bounds with the true distance nested within the bounds. The upper and lower bounds were set to $d \pm 0.5$ Å (where d is the calculated distance) for NOESY data collected in D_2O and $d \pm 1.0$ Å for NOESY data collected in H_2O. These ranges for the bounds should be free from the errors caused by ignoring indirect magnetization transfer and internal motions of the molecule.

For a methyl group, the protons were replaced by a pseudoatom located in the center of the three methyl protons, and the upper bound was modified by adding a correction term of 1.0 Å. This corresponds to the distance between the pseudoatom and any one of the three methyl protons. In a case where methylene protons are not stereospecifically assigned, a correction term corresponding to the maximum possible error was added to the upper bound. This correction term is simply the distance between the methylene protons (1.8 Å).

Structure Computations. Initial model building and structural analysis were carried out on an Evans & Sutherland PS390 color graphics system interfaced to a VAX 780 computer with MACRO-MODEL (Prof. W. C. Still, Columbia University) and INSIGHT programs (Biosym Technologies, Inc). All energy minimization and molecular dynamics calculations were carried out on a CONVEX C2 computer with the program X-PLOR (Prof. Axel Brunger, Yale University) in which all hydrogen atoms are treated explicitly. The total energy used for the energy minimizations and molecular dynamics calculations can be grouped into the empirical energy and effective energy. The empirical energy functions were taken from Brooks et al. (1983), which include covalent and nonbonded restraint terms. The effective NOE restraint potential E_{NOE} has the form of a square-well (Clore et al., 1986):

$$\begin{aligned} E_{\mathrm{NOE}} &= k_{\mathrm{NOE}}(r_{ij} - r_{ij}^{+})^2 \quad \text{if } r_{ij} > r_{ij}^{+} \\ &= 0 \quad \text{if } r_{ij}^{-} < r_{ij} < r_{ij}^{+} \\ &= k_{\mathrm{NOE}}(r_{ij} - r_{ij}^{-})^2 \quad \text{if } r_{ij} < r_{ij}^{-} \end{aligned}$$

where r_{ij}^{+} and r_{ij}^{-} are the upper and lower limits for the NOE-derived distance, respectively. r_{ij} is the distance calculated from the current calculated structures. k_{NOE} is the scale factor used for the NOE restraint potential in units of kcal mol^{-1} $\mathrm{Å}^{-2}$. Bond lengths involving hydrogen atoms were kept fixed with the SHAKE algorithm (Ryckaert et al., 1977).

Each of the initial structures was first subjected to 300 cycles of energy minimization in order to relieve bad contacts between nonbonded atoms. During this energy minimization, the hydrogen-bond constraints for DNA base pairs were used to retain Watson–Crick pairing in the DNA oligomer duplex. Another 300 cycles of restrained energy minimization with a scale factor of 2 in the NOE effective potential term was applied after all NOE distance constraints derived from NOESY spectra were inputed. The structure was then subjected to molecular dynamics refinements in two stages, namely, a high-temperature stage and a cooling/equilibration

stage. In the high-temperature stage, integration of Newton's equations of motion was performed by a Verlet (1967) integration algorithm with initial velocities assigned to a Maxwell distribution at 300 K. A loop with 10 cycles was used to gradually introduce the NOE restraints by increasing the NOE scale factor. The time step was set to be 0.0004 ps, and 250 steps dynamics were run for each NOE scale factor. The system was heated up without rescaling the velocities of the atoms at the end of each 250-step dynamics calculation, unless the temperature of the system exceeded 8000 K. In the cooling/equilibration stage, the NOE scale factor was set to be 32. Integration of Newton's equations of motion was also performed by a Verlet integration algorithm with initial velocities assigned to a Maxwell distribution at 300 K. The temperature of the system was maintained at 300 K by rescaling the velocities of the atoms every 0.250 ps. The time step of the integrator was 0.001 ps. The structure was then further refined by restrained energy minimization. The structure was repeatedly refined with combined restrained energy minimization and restrained molecular dynamics, until no single distance violation was greater than 0.2 Å.

Results

The nogalamycin numbering system is shown in structure **1**, with protons on the aglycon lacking a prime designation (for example, H3 and OH-6), protons on the nogalose ring distinguished by a prime (for example, H1′ and OCH_3-4′), and protons on the bicyclic amino sugar designated by a double prime (for example, H4″ and OH-2″). The nucleic acid sequence is numbered from the 5′-end for the d(A1-G2-C3-A4-T5-G6-C7-T8) sequence as shown schematically in structure **2**.

A1–G2–C3–A4–T5–G6–C7–T8

T8–C7–G6–T5–A4–C3–G2–A1

2

Stoichiometry and Symmetry of Complex. The self-complementary d(A1-G2-C3-A4-T5-G6-C7-T8) duplex exhibits a 2-fold element of symmetry. The addition of 2 equiv of nogalamycin to the octanucleotide duplex results in a retention of the 2-fold element of symmetry on complex formation. This is reflected in the exchangeable proton (6.5–14.0 ppm) and nonexchangeable proton 1.0–8.5 ppm) spectra of the nogalamycin–d(A-G-C-A-T-G-C-T) complex (two drugs per duplex) in 0.1 M NaCl–10 mM phosphate–aqueous buffer as shown in panels A and B of Figure 1, respectively. The proton resonances in the complex are narrow and amenable to characterization by two-dimensional NMR studies in H_2O and D_2O solution.

Exchangeable Nucleic Acid Protons in Complex. The exchangeable proton spectrum of the nogalamycin–d(A-G-C-A-T-G-C-T) complex in H_2O buffer, pH 6.7 at 25 °C (Figure 1A), exhibits three nonterminal imino proton resonances between 12.7 and 13.1 ppm and additional exchangeable resonances at 11.59 and 10.64 ppm. The imino and amino nucleic acid protons have been assigned following analysis of the NOESY (200-ms mixing time) contour plot of the complex recorded in H_2O buffer, pH 6.7 at 25 °C [Figure S1A, supplementary material (see paragraph at end of paper regarding supplementary material)].

Expanded regions of the NOESY contour plot establishing distance connectivities in the symmetrical 10.4–13.2 ppm imino and exchangeable proton region are plotted in Figure 2A and in the symmetrical 5.6–8.8 ppm amino and aromatic proton region are plotted in Figure 2B. Additional expanded NOESY contour plots establishing distance connectivities between the 10.4–13.2 ppm imino and exchangeable protons and the 5.0–8.8 ppm aromatic, sugar H1′, and amino protons are plotted in Figure 3B and between the 10.4–13.2 ppm imino and exchangeable protons and the 0.8–4.8 ppm sugar H2′,2″ and CH_3 proton region are plotted in Figure 3A. The cross-peak assignments are listed in the figure captions. The observed cross peaks permit correlation of guanosine imino with the hydrogen-bonded and exposed cytidine amino protons within a G·C pair and correlation of the thymidine imino with the adenosine H2 proton and the hydrogen-bonded and exposed adenosine amino protons within an A·T pair (see assignments in caption to Figure 3B). It should be noted that a cross peak is detected between the imino protons of flanking G2·C7 and C3·G6 base pairs (peak A, Figure 2A) but not between the imino protons of flanking C3·G6 and A4·T5 base pairs in the complex. The imino and amino nucleic acid protons assignments in the nogalamycin–d(A-G-C-A-T-G-C-T) complex at 25 °C are listed in Table I.

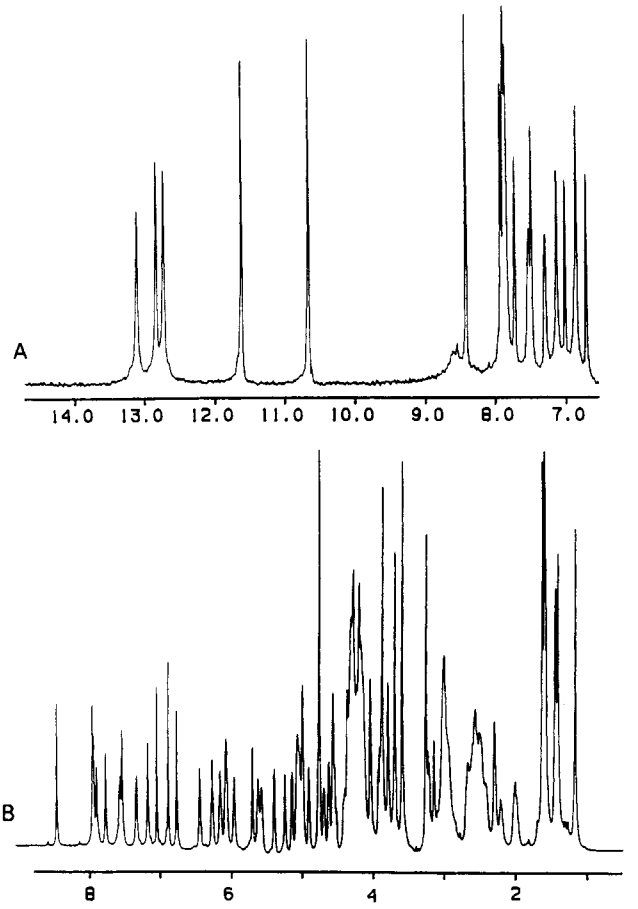

FIGURE 1: Proton NMR spectra of the nogalamycin–d(A-G-C-A-T-G-C-T) complex (two drugs per duplex) in 0.1 M NaCl–10 mM phosphate–aqueous solution. (A) Exchangeable proton spectra (6.5–14.0 ppm) in H_2O buffer, pH 6.7, 25 °C. (B) Nonexchangeable proton spectra (1.0–8.5 ppm) in D_2O buffer, pH 6.7, 30 °C.

Nonexchangeable Nucleic Acid Protons in Complex. There is excellent resolution of resonances in the nonexchangeable proton spectrum of the nogalamycin–d(A-G-C-A-T-G-C-T) complex in D_2O buffer, pH 6.7 at 30 °C (Figure 1B). The nonexchangeable nucleic acid protons have been assigned following analysis of the NOESY (200-ms mixing time) contour plot (Figure S1B, supplementary material) and the COSY contour plot of the complex in D_2O buffer, pH 6.7 at 30 °C. The cross peaks are well resolved in the NOESY

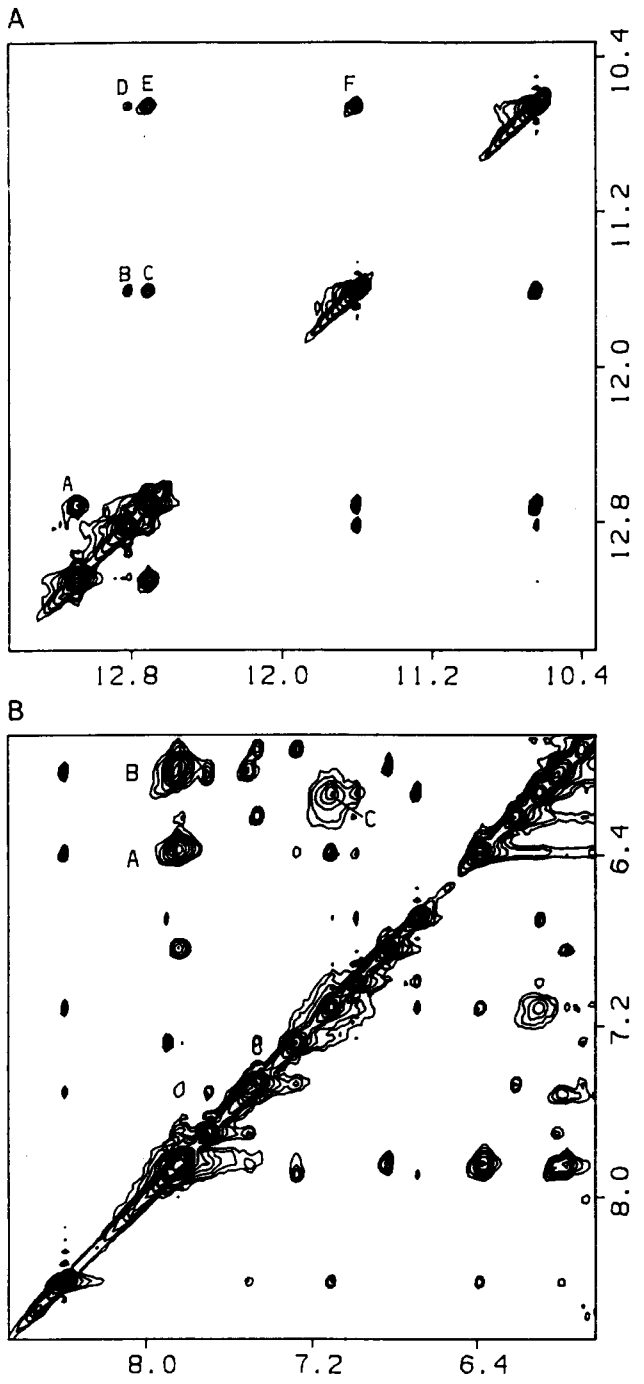

FIGURE 2: Expanded NOESY (mixing time 200 ms) contour plots of the nogalamycin–d(A-G-C-A-T-G-C-T) complex in 0.1 M NaCl, 10 mM phosphate, and H_2O, pH 6.7, 25 °C. (A) Contour plots correlating the symmetrical 10.4–13.6 ppm imino and aglycon hydroxyl proton region. Cross peaks A–F are assigned as follows: (A) G2-(NH1)–G6(NH1); (B) T5(NH3)–NOG(OH-4); (C) G6(NH1)–NOG(OH-4); (D) T5(NH3)–NOG(OH-6); (E) G6(NH1)–NOG-(OH-6); (F) NOG(OH-4)–NOG(OH-6). (B) Contour plots correlating the symmetrical 5.8–8.5 ppm base and amino proton region. Cross peaks A–C are assigned as follows: (A) C7(NH4b)–C7(NH4e); (B) C3(NH4b)–C3(NH4e); (C) A4(NH6b)–A4(NH6e).

contour plot (Figure S1B) and can be analyzed by sequential assignment procedures [Hare et al., 1983; reviewed in Patel et al. (1987), Reid (1987), and Van de Ven and Hilbers (1988)].

The distance connectivities in the NOESY contour plot between the base protons (6.9–8.5 ppm) and the sugar H1′ (5.1–6.4 ppm) and H3′ (4.5–5.1 ppm) in the complex are plotted in Figure 4A. One can trace the chain from A1 to T8 by monitoring the NOEs between the base (purine H8 or pyrimidine H6) protons and their own and 5′-flanking sugar H1′ protons (and sugar H3′ protons). We note that the cross peak between the H8 proton of G6 and the H1′ (and H3′) proton of T5 is weak in the complex recorded at a mixing time of 200 ms (designated by arrows in Figure 4A) and absent in contour plots recorded at mixing times of 100 and 50 ms (Figure S2, supplementary material). We detect NOE cross peaks between the guanosine H8 and cytidine H5 protons in the G2-C3 (peak A, Figure 4A) and G6-C7 (peak B, Figure 4A) steps in the complex. Further, NOEs are detected between the H2 proton of A4 and its own H1′ proton (peak D, Figure 4A) and the H1′ proton of T5 (peak C, Figure 4A) on the same strand but not to the H1′ proton of G6 on the partner strand in the complex.

The distance connectivities in the NOESY contour plot between the base protons (6.9–8.5 ppm) and the sugar H2′,2″ protons (1.8–3.0 ppm) in the complex are plotted in Figure 4B. The chain can be traced from A1 to T8 by noting the NOEs between the base (purine H8 or pyrimidine H6) protons and their own and 5′-flanking sugar H2″ protons (Figure 4B) and H2′ protons. An NOE is detected between the H8 proton of A4 and the CH_3 protons of T5 in the A4-T5 step (peak A, Figure 4B) in the complex.

These base and sugar H1′, H2′,2″, and H3′ proton assignments can be confirmed following analysis of other regions of the NOESY contour plot of the complex. Expanded COSY (Figure 5A) contour plots correlating H1′ (5.4–6.4 ppm) and H3′ (4.5–5.3 ppm) protons with the H2′,2″ (1.9–3.2 ppm) protons exhibit well-resolved cross peaks with the assignments listed in the figure caption. The sugar H4′ protons and some sugar H5′,5″ protons can be assigned in an analogous manner by monitoring through-space and through-bond connectivities in the complex. The base and sugar nucleic acid nonexchangeable proton assignments in the nogalamycin–d(A-G-C-A-T-G-C-T) complex at 30 °C are listed in Table I.

Comparison with Earlier Nucleic Acid Assignments. There exists a serious discrepancy between key proton assignments made in this study on the nogalamycin–d(A1-G2-C3-A4-T5-G6-C7-T8) octanucleotide complex and a previous NMR study on the nogalamycin–d(G2-C3-A4-T5-G6-C7) hexanucleotide complex (Searle et al., 1988), which share a common sequence. An examination of one-dimensional NOE data of Searle et al. (1988) for their complex in H_2O solution convinced us that they had misassigned the imino protons of C3·G6 and A4·T5 base pairs and that the assignments should be reversed. Further, they assign a chemical shift of 6.75 ppm for the H8 proton of G6 in the hexanucleotide complex while our studies unequivocally demonstrate that this proton resonates at 7.88 ppm in the octanucleotide complex. Similarly, their assignment of 7.95 ppm in the hexanucleotide complex does not agree with our assignment of 6.99 ppm in the octanucleotide complex for the H2 proton of A4. Finally, their assignment of 7.03 ppm in the hexanucleotide complex does not agree with our assignment of 6.71 ppm for the H11 proton of the nogalose sugar in the octanucleotide complex.

Nonexchangeable Nogalamycin Protons in Complex. The nonexchangeable nogalamycin protons in the nogalamycin–d(A-G-C-A-T-G-C-T) complex have been assigned following analysis of the NOESY and COSY data sets in D_2O solution.

Protons H1″, H2″, H3″, and H4″ in the bicyclic amino sugar exhibit a string of vicinal coupling connectivities in the expanded COSY spectrum (peaks A–C) of the complex in Figure 5B. The H1″ and H4″ protons could be distinguished since the CH_3-5″ protons showed a stronger NOE to H4″ than

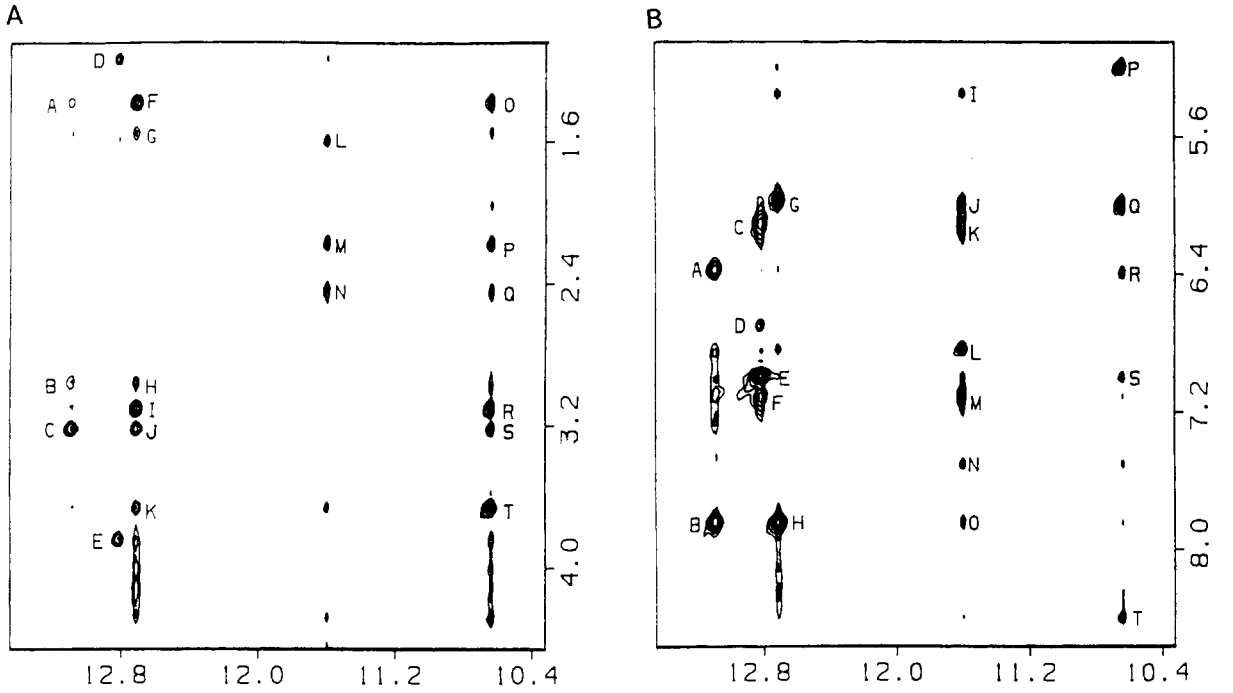

FIGURE 3: Expanded NOESY (mixing time 200 ms) contour plots of the nogalamycin–d(A-G-C-A-T-G-C-T) complex in 0.1 M NaCl, 10 mM phosphate, and H_2O, pH 6.7, 25 °C. (A) Contour plots connecting the 10.4–13.6 ppm and the 1.0–4.4 ppm regions. Cross peaks A–T are assigned as follows: (A) G2(NH1)–NOG(CH_3-3′); (B) G2(NH1)–NOG[$N(CH_3)_2$-3″]; (C) G2(NH1)–NOG(OCH_3-3′); (D) T5-(NH3)–T5(CH_3); (E) T5(NH3)–NOG($COOCH_3$-10); (F) G6(NH1)–NOG(CH_3-3′); (G) G6(NH1)–NOG(CH_3-9); (H) G6(NH1)–NOG-[$N(CH_3)_2$-3″]; (I) G6(NH1)–NOG(H2′); (J) G6(NH1)–NOG(OCH_3-3′); (K) G6(NH1)–NOG(OCH_3-2′); (L) NOG(OH-4)–NOG(CH_3-5″); (M) NOG(OH-4)–C3(H2″); (N) NOG(OH-4)–C3(H2′); (O) NOG(OH-6)–NOG(CH_3-3′); (P) NOG(OH-6)–C3(H2″); (Q) NOG(OH-6)–C3(H2′); (R) NOG(OH-6)–NOG(H2′); (S) NOG(OH-6)–NOG(OCH_3-3′); (T) NOG(OH-6)–NOG(H7). (B) Contour plots correlating the 10.4–13.6 ppm and the 5.0–8.5 ppm regions. Cross peaks A–T are assigned as follows: (A) G2(NH1)–C7(NH4e); (B) G2(NH1)–C7(NH4b); (C) T5(NH3)–A4(NH6e); (D) T5(NH3)–NOG(H11); (E) T5(NH3)–A4(H2); (F) T5(NH3)–A4(NH6b); (G) G6(NH1)–C3(NH4e); (H) G6(NH1)–C3(NH4b); (I) NOG(OH-4)–C3(H5); (J) NOG(OH-4)–C3(H1′); (K) NOG(OH-4)–A4(NH6e); (L) NOG(OH-4)–NOG(H3); (M) NOG(OH-4)–A4(NH6b); (N) NOG(OH-4)–C3(H6); (O) NOG(OH-4)–C3(NH4b); (P) NOG(OH-6)–NOG(H1′); (Q) NOG(OH-6)–C3(H1′); (R) NOG(OH-6)–A4(H1′); (S) NOG(OH-6)–A4(H2); (T) NOG(OH-6)–A4(H8).

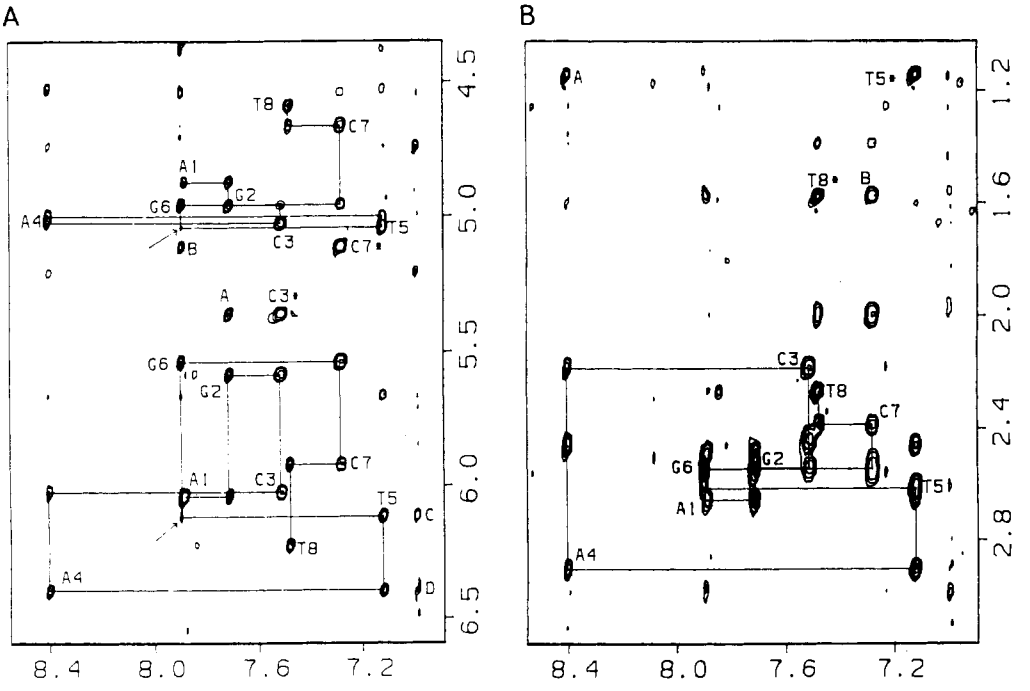

FIGURE 4: Expanded NOESY (mixing time 200 ms) contour plots of the nogalamycin–d(A-G-C-A-T-G-C-T) complex in 0.1 M NaCl, 10 mM phosphate, and D_2O, pH 6.7, 30 °C. (A) Contour plots correlating the base protons (6.9–8.5 ppm) with the sugar H1′ and H3′ protons (4.5–6.5 ppm). The cytidine H6–H5 NOEs are designated by asterisks. The lines follow the connectivities between base and sugar H1′ protons. The arrows point to weak NOEs between the H8 of G6 and the H1′ (or H3′) of T5. Cross peaks A–D are assigned as follows: (A) G2(H8)–C3(H5); (B) G6(H8)–C7(H5); (C) A4(H2)–T5(H1′); (D) A4(H2)–A4(H1′). (B) Contour plots correlating the base protons (6.9–8.5 ppm) with the sugar H2′,2″ and CH_3 protons (1.0–3.2 ppm). The thymine H6–CH_3 NOEs are designated by asterisks. The lines trace the connectivities between base and sugar H2″ protons. Cross peaks A and B are assigned as follows: (A) A4(H8)–T5(CH_3); (B) C7(H6)–T8(CH_3).

Table I: Nucleic Acid Proton Chemical Shifts in the Nogalamycin–d(A-G-C-A-T-G-C-T) Complex (Two Drugs per Duplex)[a]

	chemical shifts (ppm)										
	NH	NH_2	H8	H2	H6	H5/CH_3	H1′	H2′,2″	H3′	H4′	H5′,5″
A1			7.87	7.84			6.02	2.47, 2.65	4.86	4.23	3.75
G2	13.08		7.70				5.57	2.53, 2.53	4.94	4.32	4.13
C3		7.84, 5.98			7.49	5.34	6.01	2.43, 2.17	5.01	4.27	4.16
A4		7.11, 6.11	8.39	6.99			6.38	2.44, 2.90	4.99	4.51	4.30
T5	12.80				7.10	1.12	6.09	2.61, 2.61	5.03	4.25	4.19
G6	12.70		7.88				5.53	2.52, 2.52	4.94	4.53	4.16
C7		7.85, 6.37			7.26	5.09	5.91	1.98, 2.38	4.65	3.99	4.19, 4.10
T8					7.45	1.56	6.21	2.26, 2.26	4.58	4.00	4.09, 4.13

[a] Buffer was 0.1 M NaCl–10 mM phosphate–aqueous solution. Exchangeable proton data at 25 °C. Nonexchangeable proton data at 30 °C.

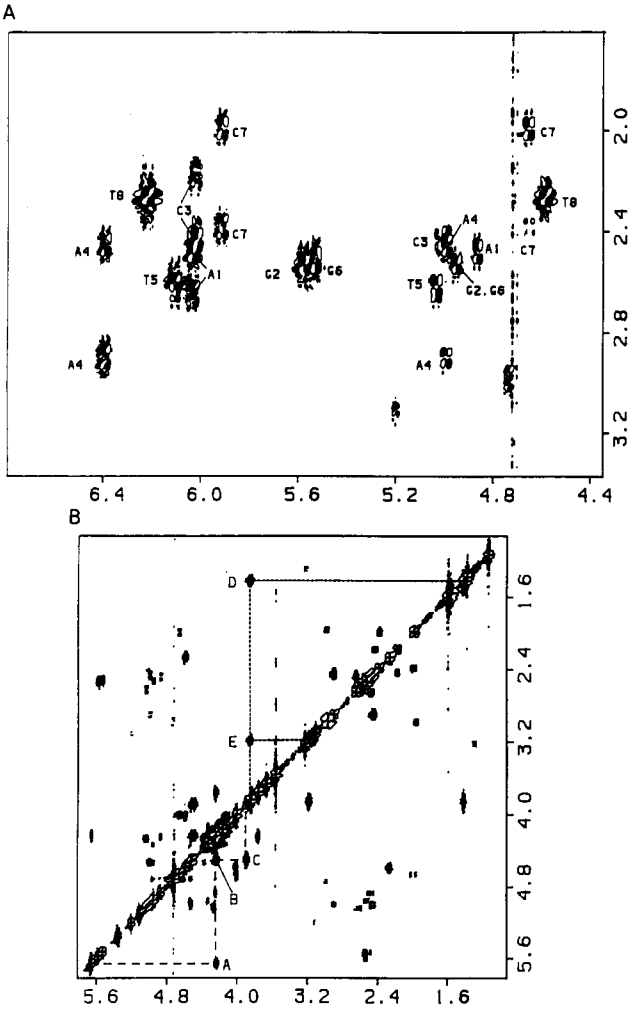

FIGURE 5: Expanded COSY contour plots of the nogalamycin–d(A-G-C-A-T-G-C-T) complex in 0.1 M NaCl, 10 mM phosphate, and D_2O, pH 6.7, 30 °C. (A) A plot correlating the sugar H1′ and H3′ protons (4.4–6.6 ppm) with the sugar H2′,2″ protons (1.8–3.3 ppm). The assignments list coupling connectivities of H2′,2″ protons with H1′ and H3′ protons. (B) A plot correlating the symmetrical 1.0–5.6 ppm region. Cross peaks A–E are assigned as follows: (A) NOG(H1″)–NOG(H2″); (B) NOG(H2″)–NOG(H3″); (C) NOG(H3″)–NOG(H4″); (D) NOG(H5′)–NOG(CH_3-5′); (E) NOG(H5′)–NOG(H4′).

to H1″. This permits assignment of the bicyclic amino protons H1″, H2″, H3″, and H4″ to resonances at 5.65, 4.22, 4.49, and 3.88 ppm, respectively, in the complex. The 2.96 ppm $N(CH_3)_2$ protons at position 3″ can be readily assigned on the basis of the very strong NOEs to the H2″, H3″, and H4″ protons on the bicyclic amino sugar.

The 6.82 ppm H3 aglycon proton exhibits an NOE to the CH_3 protons at the 5″-position and can be assigned in the

Table II: Nogalamycin Proton Chemical Shifts (ppm) in the Nogalamycin–d(A-G-C-A-T-G-C-T) Complex (Two Drugs per Duplex)[a]

aglycon ring		bicyclic amino sugar		nogalose sugar	
proton	shift	proton	shift	proton	shift
H3	6.82	H1″	5.65	H1′	5.20
OH-4	11.59	H2″	4.22	H2′	3.11
OH-6	10.64	H3″	4.49	OCH_3-2′	3.66
H7	4.72	$N(CH_3)_2$-3″	2.96	CH_3-3′	1.38
H8	2.98, 1.96	H4″	3.88	OCH_3-3′	3.22
CH_3-9	1.55	CH_3-5″	1.60	H4′	3.18
H10	4.16			OCH_3-4′	3.56
$COOCH_3$-10	3.82			H5′	3.84
H11	6.71			CH_3-5′	1.41

[a] Buffer was 0.1 M NaCl–10 mM phosphate–aqueous solution. Exchangeable proton data at 25 °C. Nonexchangeable proton data at 30 °C.

complex. The remaining aromatic proton located at 6.71 ppm is assigned by elimination to the aglycon H11 proton in the complex. The protons on the nonplanar ring A of the aglycon can be assigned by the observed sequential NOEs, starting with the H11 proton which exhibits an NOE to the 4.16 ppm H10 proton in the complex. This latter proton exhibits an NOE to the 1.55 ppm CH_3 protons at position 9 which in turn exhibits NOEs to geminal H8 protons located at 1.96 and 2.98 ppm. The remaining aglycon H7 proton at 4.72 ppm exhibits NOEs to these geminal protons, completing the assignment of the aglycon ring protons. The CH_3 protons of the $COOCH_3$ functionality at the 10-position resonate at 3.82 ppm and exhibit weak NOEs to the H7 and H10 protons in the complex.

The 3.84 ppm proton is a doublet, and this reflects a coupling between the H5′ proton and the 1.41 ppm CH_3 protons at the 5′-position on the nogalose ring in the complex. The CH_3 protons exhibit an NOE to the 3.84 ppm H5′ proton (peak D, Figure 5B) which in turn exhibits an NOE to the 3.18 ppm H4′ proton (peak E, Figure 5B) in the complex. The H4′ proton exhibits a strong NOE to the 3.56 ppm OCH_3 protons at the 4′-position on the nogalose ring. We detect NOEs between adjacent OCH_3 protons at 3.56 and 3.22 ppm, permitting assignment of the latter to position 3′ in the complex. Another set of NOEs between adjacent OCH_3 protons at 3.22 and 3.66 ppm permits assignment of the latter to the OCH_3 at the 2′-position on the nogalose ring. The OCH_3 protons at the 2′- and 3′-positions exhibit strong NOEs to the 3.11 ppm proton, which must be assigned to H2′ in the complex. The remaining nogalose proton at 5.20 ppm is assigned to H1′ since it exhibits weak NOEs to the H2′ proton and a CH_3 resonance at 1.38 ppm which is assigned to the methyl attached to the 3′-position.

This completes the assignment of the nonexchangeable nogalamycin protons in the nogalamycin–d(A-G-C-A-T-G-

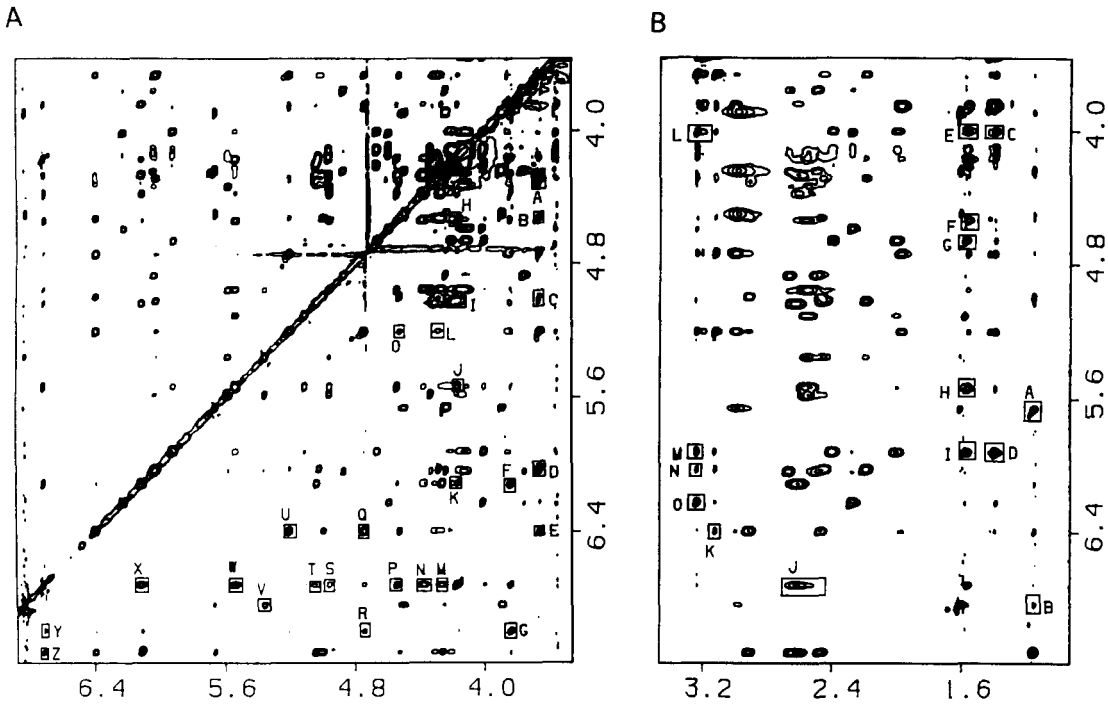

FIGURE 6: Expanded NOESY (mixing time 200 ms) contour plots of the nogalamycin–d(A-G-C-A-T-G-C-T) complex in 0.1 M NaCl, 10 mM phosphate, and D_2O, pH 6.7, 30 °C. (A) Contour plot correlating the 3.5–7.2 ppm to the 3.5–7.0 ppm region. Cross peaks A–Z correspond to intermolecular NOEs and are assigned as follows: (A) C3(H4′)–NOG(OCH_3-2′); (B) A4(H4′)–NOG(OCH_3-2′); (C) C3(H3′)–NOG(OCH_3-2′); (D) C3(H1′)–NOG(OCH_3-2′); (E) A4(H1′)–NOG(OCH_3-2′); (F) T5(H1′)–NOG($COOCH_3$-10); (G) A4(H2)–NOG($COOCH_3$-10); (H) G6(H4′)–NOG(H10); (I) T5(H3′)–NOG(H10); (J) G6(H1′)–NOG(H10); (K) T5(H1′)–NOG(H10); (L) C3(H4′)–NOG(H1′); (M) T5-(H4′)–NOG(H11); (N) G6(H5′)–NOG(H11); (O) A4(H4′)–NOG(H1′); (P) G6(H4′)–NOG(H11); (Q) A4(H1′)–NOG(H7); (R) A4-(H2)–NOG(H7); (S) G6(H3′)–NOG(H11); (T) T5(H3′)–NOG(H11); (U) A4(H1′)–NOG(H1′); (V) C3(H5)–NOG(H3); (W) G6-(H1′)–NOG(H11); (X) T5(H1′)–NOG(H11); (Y) A4(H2)–NOG(H11); (Z) T5(H6)–NOG(H11). (B) Contour plot correlating the 3.5–7.2 ppm region to the 1.0–3.4 region. Cross peaks A–O correspond to intermolecular NOEs and are assigned as follows: (A) T5(CH_3)–NOG(H1″); (B) T5(CH_3)–NOG(H3); (C) C7(H4′)–NOG(CH_3-3′); (D) C7(H1′)–NOG(CH_3-3′); (E) C7(H4′)–NOG(CH_3-9); (F) G6(H4′)–NOG(CH_3-9); (G) C7(H3′)–NOG(CH_3-9); (H) G6(H1′)–NOG(CH_3-9); (I) C7(H1′)–NOG(CH_3-9); (J) T5(H2′,2″)–NOG(H11); (K) A4(H1′)–NOG(H2′); (L) T8(H4′)–NOG(OCH_3-3′); (M) C7(H1′)–NOG(OCH_3-3′); (N) C3(H1′)–NOG(OCH_3-3′); (O) T8(H1′)–NOG(OCH_3-3′).

Table III: Intermolecular NOEs between Nogalamycin Aglycon Protons and DNA Protons in the Nogalamycin–d(A-G-C-A-T-G-C-T) Complex

nogalamycin aglycon protons	DNA protons		
	minor groove	helix axis	major groove
H3		G6(NH)	C3(NH_2b,NH_2e)
OH-4	C3(H1′,H2′,2″)	T5(NH), G6(NH)	A4(NH_2b,NH_2e) C3(H5,H6,NH_2b)
OH-6	A4(H2,H1′) C3(H1′,2″)	T5(NH), G6(NH)	A4(H8)
H11	T5(H1′,H2′,2″) G6(H1′,H4′)	T5(NH)	
H10	G6(H1′,H4′)		
$COOCH_3$-10	A4(H2), T5(H1′)	T5(NH)	
CH_3-9	G6(H1′,H4′) C7(H1′,H4′)		
H7	A4(H1′)		

Table IV: Intermolecular NOEs between Nogalamycin Sugar Protons and DNA Protons in the Nogalamycin–d(A-G-C-A-T-G-C-T) Complex

nogalamycin protons	DNA protons		
	minor groove	helix axis	major groove
bicyclic amino sugar			
H1″			T5(CH_3)
H3″			C3(NH_2b)
$N(CH_3)_2$-3″		G2(NH), G6(NH)	C3(NH_2b)
nogalose sugar			
H2′		G6(NH)	
OCH_3-2′	C3(H1′,H4′)	G6(NH)	
CH_3-3′	C7(H1′,H4′)	G2(NH), G6(NH)	
OCH_3-3′	T8(H1′)	G2(NH), G6(NH)	

C-T) complex, and the chemical shifts at 30 °C are listed in Table II.

Exchangeable Nogalamycin Protons in Complex. Two nogalamycin hydroxyl protons are detected at 11.59 and 10.64 ppm in the exchangeable proton spectrum of the nogalamycin–d(A-G-C-A-T-G-C-T) complex in H_2O buffer, pH 6.7 at 30 °C (Figure 1A). The 11.59 ppm proton is assigned to the aglycon OH at position 4 since it exhibits an NOE to the 6.82 ppm H3 proton while the 10.64 ppm proton is assigned to the aglycon OH at position 6 in the complex. The remaining hydroxyls at position 9 on the aglycon and positions 2″ and 4″ on the bicyclic amino sugar in the complex have not been identified at this time.

Intermolecular Contacts between Nogalamycin and DNA. Our ability to assign the DNA oligomer (Table I) and nogalamycin (Table II) protons in the nogalamycin–d(A-G-C-A-T-G-C-T) complex has permitted the identification and assignment of intermolecular drug–DNA NOEs in NOESY spectra recorded in H_2O and D_2O solution. A set of 52 intermolecular contacts in one symmetric half of the complex were identified in 150-ms NOESY spectra recorded in H_2O solution at 25 °C and 50-ms NOESY spectra recorded in D_2O solution at 30 °C. The intermolecular NOEs in the complex involving nonexchangeable protons are listed in the caption of Figure 6. A complete list of intermolecular NOEs appears in Tables III and IV.

The hydroxyl protons of OH-4 on aglycon ring D and OH-6 on aglycon ring B both exhibit intermolecular NOEs to the imino protons of G6 (peaks C and E, Figure 2A) and T5 (peaks B and D, Figure 2A) in the complex (Table III). These observations establish the insertion of aromatic rings B–D of the aglycon between flanking C3·G6 and A4·T5 base pairs in the complex.

Further, OH-4 located on aglycon ring D exhibits NOEs to major groove protons of C3 and A4 while OH-6 located on aglycon ring B exhibits NOEs to minor groove protons of C3 and A4 in the complex (Table III). The H11 proton of ring B on the opposite edge of the aglycon exhibits NOEs to the minor groove sugar protons of T5 and G6 in the complex (Table III). These observations require that the long axis of the aglycon be aligned approximately orthogonal to the long axis of the C3·G6 and A4·T5 base pairs with ring B positioned toward the minor groove and ring D positioned toward the major groove. Further the hydroxyl- (OH-4 and OH-6) bearing edge of the aglycon is directed toward the C3-A4 strand, and the H11-bearing edge is directed toward the T5-G6 strand in the complex.

The aglycon ring A protons (H7, CH_3-9, $COOCH_3$-10, and H11) exhibit intermolecular NOEs to minor groove base (adenosine H2) and sugar (H1′ and H4′) protons in the complex (Table III). The aglycon H7 proton at one end of ring A contacts protons of the A4 sugar while the aglycon H10 proton at the other end of ring A contacts protons on the G6 sugar, and these NOEs align the aglycon nonplanar A ring in the minor groove of the duplex.

The bicyclic amino sugar protons [H1″, H3″, and N-$(CH_3)_2$-3″] exhibit NOEs to major groove protons of C3(NH_2) and T5(CH_3) in the complex (Table IV). By contrast, the nogalose sugar protons (H2′, OCH_3-2′, CH_3-3′, and OCH_3-3′) exhibit intermolecular NOEs to the minor groove protons of C3 and C7 (H1′ and H4′) in the complex (Table IV). These intermolecular contacts position the bicyclic amino sugar in the major groove while the nogalose sugar is positioned in the minor groove on the basis of the intermolecular NOEs detected in the complex.

Experimental Distance Bounds. We have outlined under Materials and Methods the approach used to define lower and upper bounds for proton pairs with a detectable NOE between them in the NOESY spectra at short mixing times of the nogalamycin–d(A-G-C-A-T-G-C-T) complex. The volume integrals for NOE cross peaks were measured for a NOESY data set on the complex recorded at a mixing time of 50 ms in D_2O solution and a related NOESY data set on the complex recorded at a mixing time of 150 ms in H_2O solution. A set of distance bounds corresponding to the 52 intermolecular distance contraints is listed in Table V. These 52 intermolecular distance bounds along with 137 constraints between nucleic acid protons and 45 constraints between nogalamycin protons in the complex were incorporated in the molecular dynamics simulation and correspond to a total of 234 constraints for one symmetrical half of the nogalamycin–d(A-G-C-A-T-G-C-T) complex.

Starting Models for Structure Refinement. The d(A-G-C-A-T-G-C-T) duplex was generated with a standard B-form structure by use of the MACRO-MODEL program (Prof. W. C. Still, Columbia University). The previously published coordinates of nogalamycin from a crystallographic analysis (Arora, 1983) were used to generate the drug. The nogalamycin was intercalated into the duplex at (C-A)·(T-G) sites with the bicyclic amino and nogalose sugars positioned in the major and minor grooves, respectively, and the aglycon hydroxyls directed toward the C3-A4 strand as established in a previous section. Two quite different intial structures of the complex were generated for the molecular dynamics computations as a test for the convergence characteristics of the final refined structures. One initial structure, Init-A, was built by simply inserting two nogalamycins at symmetrically related sites on the B-form d(A-G-C-A-T-G-C-T) duplex without increasing the distance between base pairs at the (C-A)·(T-G) intercalation sites (Figure 7A). The other initial structure, Init-B, was built by first separating the base pairs at the (C-A)·(T-G) binding site on the octamer duplex and then intercalating the nogalamycins between the separated C3·G6 and A4·T5 base pairs such that the nogalamycin is positioned closer to the T5-G6-C7 strand (Figure 7B). There are bad contacts between the base pairs and the aglycon ring in the Init-A structure and bad contacts between the sugar–phosphate backbone and the nogalose ring in the Init-B structure of the complex. Both starting structures have very high van der Waals energy at the level of 10^9 kcal and exhibit a root-mean-square deviation of 7.8 Å for all heavy atoms between these structures.

Table V: Distance Bounds between Nogalamycin and d(A-G-C-A-T-G-C-T) Nonexchangeable Protons in the Complex and Their Comparison with Observed Distances in the NMR–Molecular Dynamics Refined Structure of the Complex

intermolecular proton pairs	distance bounds (Å)	actual distance (Å)
C3(H4′)–NOG(OCH_3-2′)	2.2–4.2	2.8
C3(H1′)–NOG(OCH_3-2′)	2.2–4.2	2.7
A4(H2)–NOG($COOCH_3$-10)	2.6–4.6	2.7
A4(H1′)–NOG(H7)	2.5–3.5	2.5
T5(CH_3)–NOG(H1″)	2.4–4.4	2.5
T5(H1′)–NOG(H11)	3.1–4.1	3.1
T5(H2′)–NOG(H11)	2.6–3.6	3.7
T5(H2″)–NOG(H11)	2.6–3.6	2.6
T5(H1′)–NOG($COOCH_3$-10)	3.2–5.2	3.4
G6(H1′)–NOG(H11)	2.9–3.9	3.9
G6(H4′)–NOG(H11)	3.5–4.5	3.8
G6(H1′)–NOG(H10)	2.3–3.3	3.4
G6(H4′)–NOG(H10)	2.0–2.8	2.3
G6(H1′)–NOG(CH_3-9)	2.5–4.0	3.6
G6(H4′)–NOG(CH_3-9)	2.8–4.8	3.8
C7(H1′)–NOG(CH_3-9)	3.5–5.5	3.6
C7(H1′)–NOG(CH_3-3′)	2.1–4.1	2.8
C7(H4′)–NOG(CH_3-9)	2.4–4.4	2.8
C7(H4′)–NOG(CH_3-3′)	2.6–4.6	4.3
T8(H1′)–NOG(OCH_3-3′)	2.7–4.7	4.1

Structure Refinement. The initial structures served as starting models for structure refinement using molecular dynamics (MD) computations with NMR-based distance bounds as input constraints. The refinement protocol is outlined under Materials and Methods and was judged to be complete when no single distance violation was greater than 0.2 Å. The final structures which were refined from two quite different starting structures are superimposed on the basis of a best fit for all heavy atoms in Figure 7C and exhibit a root-mean-square deviation of 0.6 Å.

One of these final structures for the nogalamycin–d(A-G-C-A-T-G-C-T) complex is plotted in stereo in Figure S3A (supplementary material) and with the nogalamycins removed to emphasize the intercalation cavity in Figure S3B (supplementary material). The intermolecular interproton distances measured for this structure of the complex show good agreement with the input experimental distance bounds used in the molecular dynamics calculation (Tables V and VI).

Structural Features of NMR–MD-Refined Complex. The nogalamycin–d(A-G-C-A-T-G-C-T) complex (two drugs per

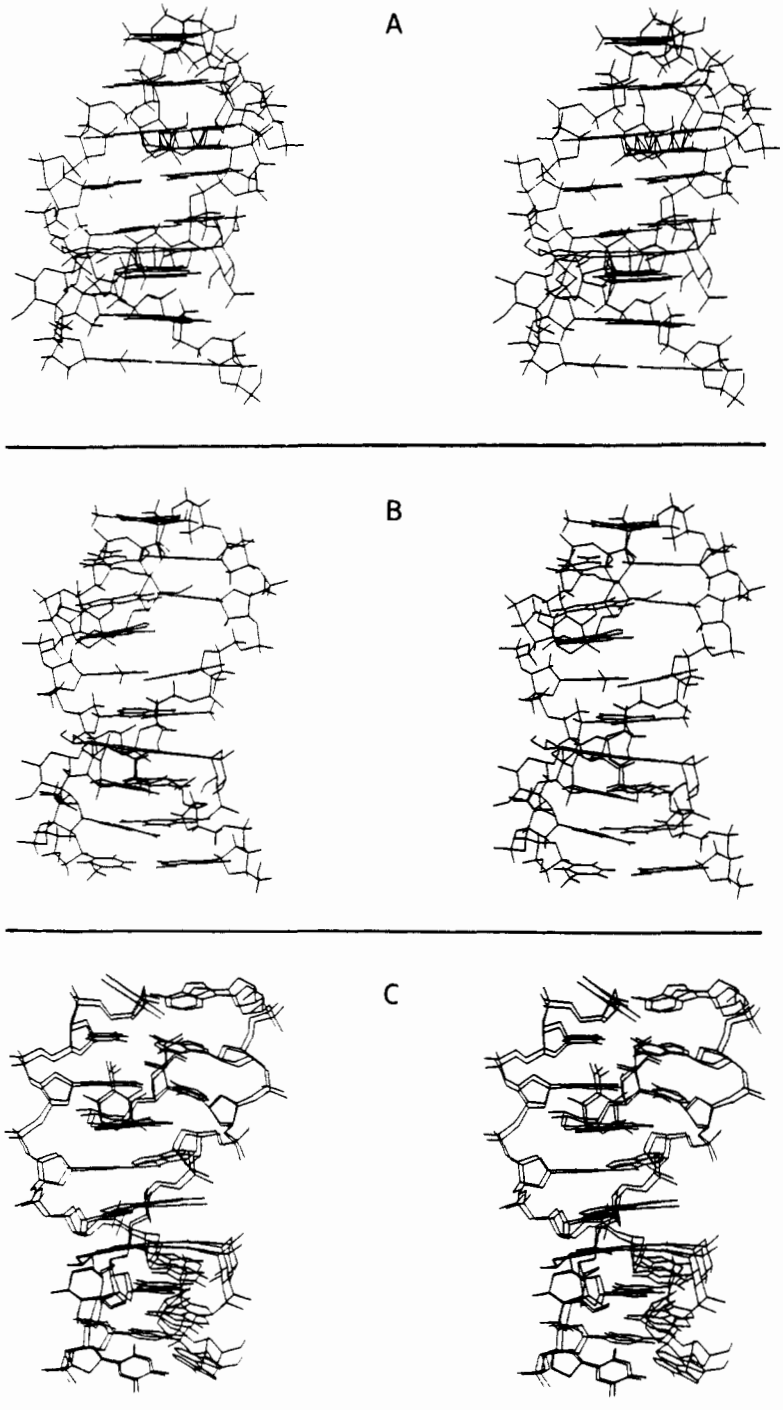

FIGURE 7: Stereoviews of the initial structures of the nogalamycin–d(A-G-C-A-T-G-C-T) complex (two drugs per duplex) used as starting models in the molecular dynamics refinements with NMR distance constraints. (A) Init-A structure. The nogalamycin aglycon was intercalated into the d(C-A)·d(T-G) step without separation of C3·G6 and A4·T5 base pairs. The aglycon rings are approximately positioned along the helix axis. (B) Init-B structure. The nogalamycin aglycon was intercalated into the d(C-A)·d(T-G) step between separated C3·G6 and A4·T5 base pairs. The aglycon ring is positioned closer to the T5-G6-C7 strand. (C) A stereoview of two superpositioned structures of the nogalamycin–d(A-G-C-A-T-G-C-T) complex (two drugs per duplex) following molecular dynamics refinement including NMR-based distance constraints. These refined structures were generated from Init-A and Init-B starting structures.

duplex) exhibits 2-fold symmetry with nogalamycins intercalated at symmetry-related d(C3-A4)·d(T5-G6) steps (Figure S3). The two nogalamycin molecules intercalate back-to-back into the d(A-G-C-A-T-G-C-T) duplex with the nogalose and bicyclic amino sugars positioned on the same side of the chromophore ring and directed toward the ends of the duplex (Figure S3).

Stereoviews of the complexation site (Figure 8A) emphasize the wedge-shaped orientation of the base pairs at the intercalation site (Figure 9A) and the selective stacking of the aglycon with one strand (T5-G6) and not the other (C2-A3) (Figure 9B), as well as the relative orientation and intermolecular contacts between the sugars at either end of the aglycon and the grooves of the DNA (Figure 8A). The bicyclic amino sugar is positioned in the major groove, and the view looking into the major groove at the intercalation site is shown in Figure 10B. The nogalose sugar is positioned in the minor groove, and the view looking into the minor groove at the intercalation site is shown in Figure 10A. The nogalose sugar fills the expanded minor groove with close van der Waals contacts between the nogalose and DNA sugars in the complex (Figure 8B).

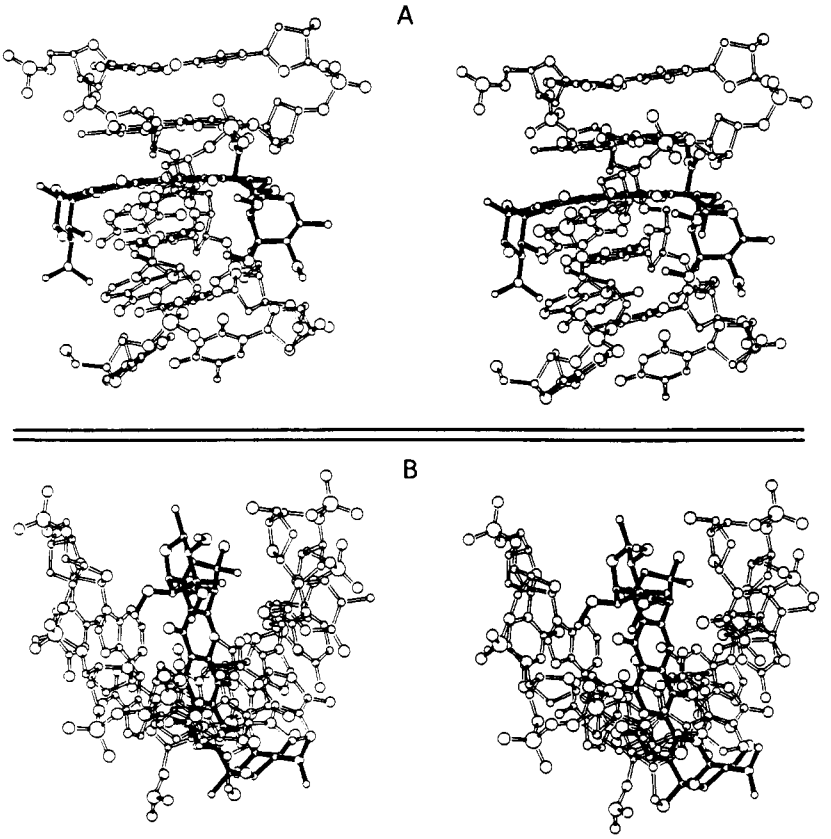

FIGURE 8: Stereoviews of the complexation site [drug and (A4-T5-G6-C7-T8)·(A1-G2-C3-A4-T5) pentanucleotide segment] in the nogalamycin–d(A-G-C-A-T-G-C-T) complex (two drugs per duplex). (A) View emphasizing the position of the nogalose sugar in the minor groove and the position of the bicyclic amino sugar in the major groove. (B) View emphasizing the positioning of the aglycon A ring and the nogalose sugar within the walls of the minor groove.

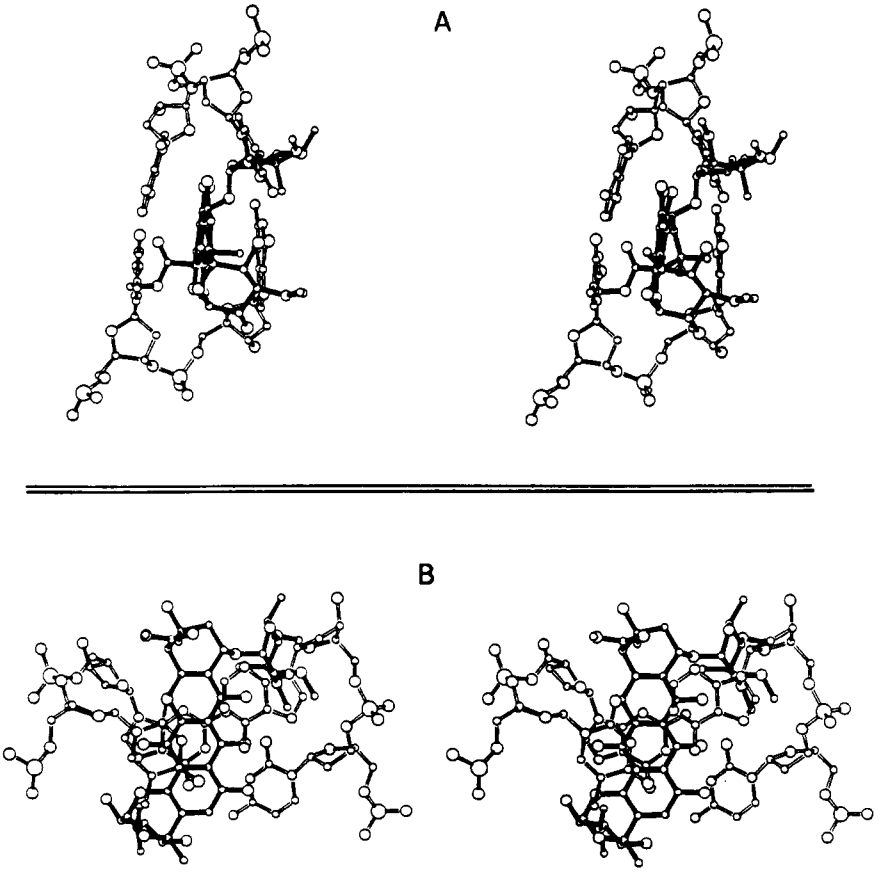

FIGURE 9: Stereoview of the intercalation site (drug and adjacent base pairs) in the nogalamycin–d(A-G-C-A-T-G-C-T) complex (two drugs per duplex). (A) This drawing emphasizes the buckling of the base pairs at the intercalation site. (B) This drawing emphasizes the overlap geometries between the aglycon and flanking base pairs.

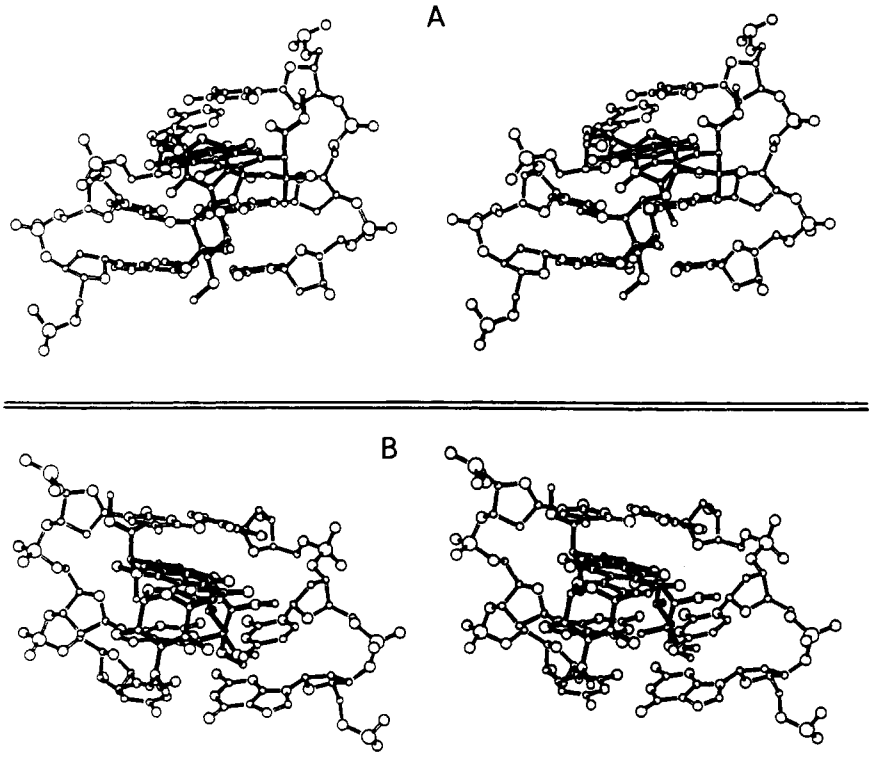

FIGURE 10: Stereoviews of the intercalation site [drug and (G2-C3-A4)·(T5-G6-C7) trinucleotide segment] in the nogalamycin–d(A-G-C-A-T-G-C-T) complex (two drugs per duplex). (A) View into the minor groove. (B) View into the major groove.

Table VI: Distance Bounds between Nogalamycin and d(A-G-C-A-T-G-C-T) Exchangeable Protons in the Complex and Their Comparison with Observed Distances in the NMR–Molecular Dynamics Refined Structure of the Complex

intermolecular proton pairs	distance bounds (Å)	actual distance (Å)
G2(NH1)-NOG[$N(CH_3)_2$-3″]	2.5–5.0	4.5
G2(NH1)-NOG(CH_3-3′)	2.7–5.2	4.6
G2(NH1)-NOG(OCH_3-3′)	2.2–4.7	4.8
C3(H6)-NOG(OH-4)	2.7–4.7	4.2
C3(H5)-NOG(OH-4)	2.6–4.6	4.5
C3(H1′)-NOG(OH-4)	2.0–4.0	3.3
C3(H1′)-NOG(OH-6)	2.0–3.9	3.1
C3(H2″)-NOG(OH-4)	2.4–4.4	3.3
C3(H2′)-NOG(OH-4)	2.4–4.4	4.4
C3(H2″)-NOG(OH-6)	2.4–4.4	4.4
C3(NH4b)-NOG(OH-4)	2.6–4.6	4.6
C3(NH4b)-NOG(H3″)	2.5–4.5	3.6
C3(NH4b)-NOG(H3)	2.3–4.3	3.2
C3(NH4e)-NOG(H3)	2.1–4.1	3.2
C3(NH4b)-NOG[$N(CH_3)_2$-3″]	2.3–4.8	4.6
A4(H8)-NOG(OH-6)	2.3–4.3	3.8
A4(NH6b)-NOG(OH-4)	2.0–4.0	3.4
A4(H2)-NOG(OH-6)	2.7–4.7	4.6
A4(H1′)-NOG(OH-6)	2.3–4.3	4.3
A4(NH6e)-NOG(OH-4)	2.0–3.9	3.4
T5(NH3)-NOG($COOCH_3$-10)	2.2–5.2	5.1
T5(NH3)-NOG(OH-4)	2.7–4.7	4.7
T5(NH3)-NOG(OH-6)	2.8–4.8	4.6
T5(NH3)-NOG(H11)	2.4–4.4	4.2
G6(NH1)-NOG(OH-4)	2.5–4.5	3.9
G6(NH1)-NOG(OH-6)	2.4–4.4	4.4
G6(NH1)-NOG(H3)	2.6–4.6	4.6
G6(NH1)-NOG(OCH_3-3′)	2.4–4.9	4.0
G6(NH1)-NOG[$N(CH_3)_2$-3″]	2.5–5.0	4.7
G6(NH1)-NOG(CH_3-3′)	2.2–4.7	4.2
G6(NH1)-NOG(H2′)	2.4–4.4	4.4
G6(NH1)-NOG(OCH_3-2′)	2.5–5.0	5.0

Nogalamycin Monomer Conformation in Complex. The aglycon ring of nogalamycin contains planar aromatic rings B–D and nonplanar ring A. The NMR distance and coupling connectivities as reflected in the NMR–MD-refined structure establish that aglycon ring A adopts a half-chair conformation such that C9 is out the plane of the aglycon aromatic ring system and on the same side as the nogalose and bicyclic amino sugar rings. The $COOCH_3$ group at position 10 and the OH group at position 9 adopt axial and equatorial positions, respectively. The nogalose and bicyclic amino sugars both adopt chair conformations in the complex. The OH-2″ and OH-4″ protons on the bicyclic sugar are directed toward the helix axis as are the CH_3-3′ protons on the nogalose sugar. The nogalose and bicyclic amino sugars are on the same side of the aglycon (Figure 8A) and are directed toward either end of the duplex in the complex (Figure S3).

We can compare the conformation of free nogalamycin in the crystalline state (Figure S5A) (Arora, 1983) with that of nogalamycin in the complex determined in this study in solution (Figure S5B). It is apparent that the bicyclic amino sugar and the nogalose sugar are both pulled toward each other in the direction of the helix axis for nogalamycin on DNA complex formation in solution (compare panels B and A of Figure S5). This conformational transition on complex formation is achieved by changes in the torsion angles C7–O7 (14°) and O7–C1′ (16°) that link aglycon ring A with the nogalose sugar. This movement of the nogalose and bicyclic amino sugars must be associated with optimizing the van der Waals and hydrogen-bonding drug–nucleic acid contacts that stabilize the complex in solution.

DNA Conformation in the Complex. A qualitative examination of the experimental NOE data establishes that the A·T and G·C pairs adopt Watson–Crick alignment and the glycosidic torsion angles are in the anti range in the nogalamycin–d(A-G-C-A-T-G-C-T) complex. This is confirmed by an examination of the glycosidic torsion angle values for the NMR–MD solution structure of the complex.

Conformational features of the (C3-A4)·(T5-G6) intercalation site in the complex are of special interest. We note that the C3·G6 and A4·T5 base pairs are buckled such that the

intercalation site is wedge-shaped at the C3-A4 step in contrast to the T5-G6 step where the bases are parallel to each other (Figures 9A and S4A). This is reflected in the interproton separations between the base proton and the 5′-flanking sugar H1′ and H3′ protons at the C3-A4 and G5-T6 steps centered about the intercalation site in the complex. Thus, the G6(H8) to T5(H1′) and T5(H3′) separations are 6.9 and 6.3 Å, respectively, in the T5-G6 step in the complex. By contrast, the A4(H8) to C3(H1′) and C3(H3′) separations are 3.7 and 4.2 Å, respectively, in the C3-A4 step in the complex. Further, the C3·G6 and A4·T5 pairs that flank the intercalation site are sheared relative to each other so that T5 and G6 are positioned over each other while C3 and A4 are displaced relative to each other (Figures 9B and S4B).

We detect a widening of the minor groove (phosphorus–phosphorus cross-strand separation ranges between 15 and 16 Å) at the nogalose sugar binding site spanning (G6-C7)·(G2-C3) steps in the complex. This minor groove expansion is localized since it does not propagate to the central (A4-T5)·(A4-T5) steps in the complex.

Overlap Geometry at Intercalation Site in Complex. The alignment of the aglycon chromophore and the overlap geometries with respect to the flanking C3·G6 and A4·T5 base pairs in the NMR–MD-refined structure reflects the observed intermolecular NOEs observed experimentally between the aglycon and nucleic acid residues defining the intercalation site. The aglycon ring is aligned orthogonal to the direction of the long axis of the base pairs with ring A directed toward the minor groove (Figure 9B). Aglycon ring C stacks directly over the six-membered ring of G6 while aglycon ring A shows no overlap with flanking base pairs in the complex. The aromatic rings of the aglycon predominantly stack over the bases in the T5-G6 step with the OH-4 and OH-6 protons positioned close to the helix axis and pointed in the direction of the C3-A4 step (Figure 9B).

Intermolecular Contacts in the Minor Groove. The aglycon A ring and nogalose sugar of nogalamycin are positioned in the minor goove of the duplex with the intermolecular alignments stabilized by a large set of van der Waals contacts. We first outline intermolecular contacts involving aglycon functional groups and then those involving nogalose functional groups.

The H10 and H11 protons are on the aglycon edge directed toward the T5-G6 step and are aligned between sugar protons of T5 and G6 in the complex. The $COOCH_3$-10 group is the only functionality that is directed toward and interacts with the A4·T5 pair. The methyl group is positioned toward the H2 of A4 and the H1′ of T5 of the A4-T5 step while the carbonyl group may be linked through a bridging water molecular to the N3 ring nitrogen of A4. The $COOCH_3$-10 functionalities from the two bound nogalamycins in the complex are directed toward each other with the closest approach involving their methyl groups. The aglycon CH_3-9 group adopts an axial orientation and forms a hydrophobic patch which includes the nogalose H5′ proton and CH_3-3′ group. The CH_3-9 protons are positioned between the minor groove edge and sugar ring of G6 in the complex. The OH-9 and geminal CH_2-8 protons are directed toward solvent with the OH-9 not participating in intermolecular hydrogen-bond formation. The aglycon H7 proton and nogalose sugar H1′ proton are positioned between the minor groove edge and sugar ring of A4 in the complex.

The nogalose sugar ring in the chair conformation is sandwiched between the walls of the widened minor groove with one face (CH_3-3′ and H5′) directed toward the G6-C7 sugar–phosphate backbone while the opposite face (OCH_3-3′ and OCH_3-4′) is directed toward the G2-C3 sugar–phosphate backbone in the complex. The nogalose H2′ proton is directed toward the minor groove of the C3·G6 pair while the OCH_3-2′ group interacts with the C3 sugar in the complex. The H4′ proton and OCH_3-4′ and CH_3-5′ groups are pointing out toward solvent and do not contact the DNA in the complex. The CH_3-3′ group is directed toward the minor groove and is proximal to the sugar rings in the G6-C7 step.

Two potential intermolecular hydrogen bonds can be formed between the nogalose sugar and the minor groove edge of the (G2-C3)·(G6-C7) segment in the NMR–MD structure of the complex. The ether oxygen of the nogalose OCH_3-3′ group can form an intermolecular hydrogen bond with the exposed 2-amino group of G2 (2.22 Å) in the complex. A second intermolecular hydrogen bond can be formed between the O7 atom that links aglycon ring A with the nogalose sugar and the exposed amino proton of G6 (2.06 Å) in the complex. These pairs of intermolecular hydrogen bonds involving 2-amino protons on adjacent guanosines G2 and G6 on partner strands emphasize the importance of the sequence (G2-C3-A4)·(T5-G6-C7) for intercalation of nogalamycin at its preferred (C-A)·(T-G) site on duplex DNA. It should be noted the nogalose sugar and aglycon ring A along with the $COOCH_3$-10 side chain constitute a continuous domain that interacts with the minor groove edge of the three base pair (G2-C3-A4)·(T5-G6-C7) segment in the complex.

Intermolecular Contacts in the Major Groove. The bicyclic amino sugar in the chair conformation which is fused to aglycon ring D is positioned in the major groove. The bicyclic amino sugar forms fewer van der Waals intermolecular contacts with the DNA since it is not sandwiched between the walls of the major groove in the complex.

The H3 proton on aglycon ring D is stacked over the NH_2 group of C3 in the complex. The H1″ and CH_3-5″ bridgehead protons are directed toward the CH_3 group of T5, forming an intermolecular hydrophobic patch in the complex. This observation clarifies the role of thymidine in the sequence selectivity of nogalamycin for intercalation at (C-A)·(T-G) steps on DNA. The bicyclic amino sugar H3″ proton in an axial orientation points toward the major groove edge of the C3·G6 pair while the charged $N(CH_3)_2$-3″ group in an equatorial orientation is positioned in the major groove between the edges of the C3·G6 and G2·C7 base pairs in the complex.

Two potential intermolecular hydrogen bonds can be formed between the bicyclic amino sugar and the major groove edge of the C3·G6 pair in the NMR–MD structure of the complex. The OH-2″ and OH-4″ hydroxyl protons are directed toward the major groove edge of the C3·G6 pair and form intermolecular hydrogen bonds with N7 (2.01 Å) and O6 (2.31 Å) atoms of G6, respectively. These observations emphasize the importance of the major groove edge of guanosine in stabilizing the complex formed following intercalation at the (C-A)·(T-G) step in duplex DNA.

Discussion

Spectral Markers. The analysis of the two-dimensional data sets permits a virtually complete assignment of exchangeable and nonexchangeable DNA (Table I) and drug (Table II) protons in the nogalamycin–d(A-G-C-A-T-G-C-T) complex. This provides markers located on the aglycon, the bicyclic amino sugar, and the nogalose sugar of the nogalamycin which together with the corresponding intermolecular NOEs define the complementarity of the fit between the drug and the DNA.

This study provides a good example of the wealth of additional information available following analysis of ex-

changeable proton data and the NOEs between these protons and nearby exchangeable and nonexchangeable protons in the nogalamycin–d(A-G-C-A-T-G-C-T) complex. This is best illustrated by the exchangeable 11.59 ppm OH-4 and 10.64 ppm OH-6 aglycon protons which exhibit a large number of intra- and intermolecular NOEs (peaks B–F, Figure 2A; peaks L–T, Figure 3A; peaks I–T, Figure 3B) in the complex (Table III). By contrast, we were unable to detect the bicyclic amino sugar OH-2″ and OH-4″ protons and aglycon OH-9 protons, presumably due to their proximity to the solvent water resonance.

The nucleic acid imino protons of the nonterminal base pairs along with the hydrogen-bonded and exposed amino protons of the nonterminal cytidines C3 and C7 (peaks A and B, Figure 2B) and adenosine A4 (peak C, Figure 2B) are detected in exchangeable proton spectra of the complex. By contrast, the amino protons of guanosines G2 and G6 could not be identified, presumably due to broadening associated with intermediate rotation rates about the C–NH_2 bond of the guanosines in the complex.

Previous Research on Nogalamycin–DNA Complexes. An earlier two-dimensional NMR study reported on the proton resonance assignments and intermolecular NOEs in the nogalamycin–d(G2-C3-A4-T5-G6-C7) complex in aqueous solution (Searle et al., 1988). This study defined the stacking geometry at the intercalation site in the complex and positioned the nogalose and bicyclic amino sugars in the minor and major grooves of DNA, respectively. This group also proposed potential intermolecular hydrogen bonds and van der Waals contacts associated with complex formation (Searle et al., 1988). Our research on the nogalamycin–d(A1-G2-C3-A4-T5-G6-C7-T8) complex has expanded on the earlier contribution in three important ways. (1) We have identified and corrected proton assignments reported in the earlier study (Searle et al., 1988) for critical proton markers on the C3·G6 and A4·T5 base pairs that flank the intercalation site (see Results). (2) Our NMR studies have emphasized the importance of intermolecular NOEs involving exchangeable protons in defining the conformation of the nogalamycin–DNA oligomer complex. The large number of intermolecular NOEs in the complex (Table III) deduced from our two-dimensional NOESY data sets in H_2O (Figure S1A) contrasts with the limited and partially misinterpreted one-dimensional NOE data on the complex in H_2O reported by Searle et al. (1988). (3) The earlier NMR research on the nogalamycin–DNA oligomer complex was limited to qualitative conclusions since Searle et al. (1988) did not attempt to measure interproton distance bounds and analyze them with structure reconstruction algorithms. By contrast, our use of NMR distance contraints as input parameters in a molecular dynamics computation has yielded a detailed three-dimensional view of the intermolecular interactions that account for the sequence specificity and stability of nogalamycin bound to (G-C-A)·(T-G-C) sites on duplex DNA.

Two crystallographic studies have been reported on the nogalamycin–d(*C-G-TsA-*C-G) complex (two drugs per duplex) where *C is either C or me^5C (Liaw et al., 1989; Williams et al., 1990). These crystallographic studies provide details of the complex at atomic resolution and independently establish both the aglycon intercalation site geometry and the nogalamycin sugar–DNA groove interactions. The aglycon of nogalamycin intercalates at (C-G)·(C-G) steps with the nogalose and bicyclic sugars directed toward the center of the duplex in the nogalamycin–d(*C-G-TsA-*C-G) complex in the crystal (**3**) (Liaw et al., 1989; Williams et al., 1990). By contrast, the aglycon intercalates at (C-A)·(T-G) steps with the nogalose and bicyclic amino sugars directed toward the ends of the helix in the nogalamycin–d(G-C-A-T-G-C) complex (Searle et al., 1988) and in our studies of the nogalamycin–d(A-G-C-A-T-G-C-T) complex in solution (**4**). Thus, even though intercalation occurs at a common pyrimidine-(3′–5′)purine step, the nogalamycin sugar side chains point in opposite directions for the complex studied in the crystal (**3**) compared to those in the complex studied in solution (**4**). The different orientations could reflect the fact that the intercalation sites are separated by four base pairs in the DNA sequences used in crystallographic studies and are separated by two base pairs in DNA sequences used for NMR studies in solution.

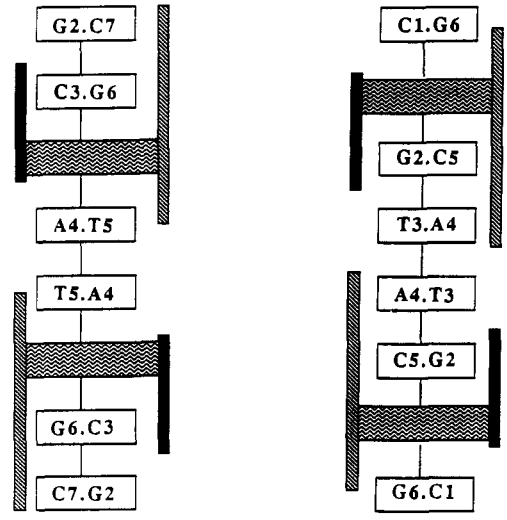

3 **4**

Sequence Specificity. The experimental NMR data establish that 2 equiv of nogalamycin binds to the self-complementary d(A-G-C-A-T-G-C-T) duplex as monomers through intercalation of the aglycons at symmetry-related (C3-A4)·(T5-G6) steps on complex formation. The observed sequence specificity is consistent with footprinting studies that identified (C-A)·(T-G) as the preferred nogalamycin binding site in restriction fragments (Fox & Waring, 1986; White & Phillips, 1989) and with an earlier NMR study on a DNA oligomer duplex (Searle et al., 1988).

Our studies and those of Searle et al. (1988) strongly establish that the three base pair segment with sequence (G-C-A)·(T-G-C) is a strong recognition site for nogalamycin on duplex DNA. This specificity is associated in our study with the intermolecular hydrogen bonds between the nogalose sugar and the 2-amino group of G2 and G6 in the minor groove and the intermolecular hydrogen bonds between the bicyclic amino sugar and the O6 and N7 of G6 in the major groove at the (G2-C3-A4)·(T5-G6-C7) steps in the nogalamycin–d(A-G-C-A-T-G-C-T) complex in solution. Further, the CH_3 group of T5 is involved in an intermolecular hydrophobic patch with the bicyclic amino sugar protons of nogalamycin, which contributes to the recognition and stability of the complex.

The three base pair recognition element is spanned in the minor groove by the structural motif which includes the $COOCH_3$-10 group, the aglycon ring A in a half-chair conformation, and the nogalose ring in a chair conformation. This nogalamycin domain adopts a handedness that complements the handedness of the minor groove and results in critical van der Waals contacts with the walls of this groove. Our studies establish that the specificity of nogalamycin for the (G-C-

A)·(T-G-C) sequence in the d(A-G-C-A-T-G-C-T) duplex is associated with intermolecular van der Waals and hydrogen-bonding contacts in both the minor and major grooves.

The nogalamycin molecule adopts a dumbbell-shaped structure with bulky sugar ligands at either end of the aglycon ring (Arora, 1983). It is likely, as has been suggested (Liaw et al., 1989; Williams et al., 1990), that the DNA duplex must locally denature prior to intercalation of the aglycon ring, and this may be facilitated by the presence of at least one A·T base pair flanking the intercalation site. We have established the importance of G2 and G6 for intermolecular hydrogen-bond formation and of T5 for intermolecular van der Waals contacts, and this together with the possible requirement for at least one A·T pair explains the sequence specificity of nogalamycin for (G2-C3-A4)·(T5-G6-C7) steps on the d(A-G-C-A-T-G-C-T) duplex.

Intermolecular Contacts Stabilizing Complex. Nogalamycin is unique among intercalating antitumor agents in that the complex is stabilized by drug chromophore–DNA base pair stacking interactions, as well as complementary intermolecular drug sugar–DNA groove interactions in both the minor and major grooves.

The nogalose and bicyclic amino sugars which are covalently attached to opposite sides of the aglycon chromophore project in the same direction relative to the plane of the aglycon ring (Arora, 1983). Thus, the stacking arrangement of the aglycon between base pairs will be dictated by the complementary interactions between the nogalose sugar and the minor groove and between the bicyclic amino sugar and the major groove. We note that the aglycon ring does stack with adjacent pairs at the intercalation site but the stacking is predominantly with one strand (the T5-G6 step) and not the other (the C3-A4 step) (Figure 9B). This results in a wedge-shaped intercalation site which is compressed at the C3-A4 step (Figure 9A). The base pairs at the intercalation site are also sheared relative to each other so that T5 and G6 are stacked while C3 and A4 are unstacked in a view down the helix axis (Figure 9B). These features of aglycon–base pair stacking along one strand and the shearing of base pairs at the intercalation site are common to the structure of the nogalamycin–d(A-G-C-A-T-G-C-T) complex in solution (Figure 9) and the nogalamycin–d(*C-G-TsA-*C-G) complex in the crystalline state (Liaw et al., 1989; Williams et al., 1990).

The guanosine residues in the nogalamycin–d(A-G-C-A-T-G-C-T) complex play a critical role in being both donors and acceptors in intermolecular hydrogen-bond formation. The minor groove 2-amino protons of both G2 and G6 donate hydrogen bonds to acceptors on the nogalose sugar residue and align the nogalose ring within the walls of the minor groove in the complex. The importance of the intermolecular hydrogen bonds involving the guanosine 2-amino protons has previously been documented for actinomycin complexes with dG (Sobell et al., 1971) and with d(G-C) (Takusagawa et al., 1982) in the crystalline state and in the metal ion coordinated chromomycin dimer–DNA oligomer complex in solution (Gao & Patel, 1989a,b).

The major groove O6 and N7 atoms of G6 can accept hydrogen bonds from hydroxyl groups on the bicyclic amino sugar in the nogalamycin–d(A-G-C-A-T-G-C-T) complex. We propose that these two adjacently aligned intermolecular hydrogen bonds are critical for positioning the bicyclic amino sugar of nogalamycin in the major groove. Most drugs studied to date involve minor groove DNA recognition so that the extension of the specific intermolecular hydrogen-bonding interactions observed in the major groove in the nogalamycin–DNA complex to other systems cannot be evaluated at this time. A direct comparison of the intermolecular hydrogen-bonding interactions observed in the nogalamycin–d(A-G-C-A-T-G-C-T) complex in solution (**4**) with those observed in the nogalamycin–d(*C-G-TsA-*C-G) complex (**3**) in the crystalline state cannot be undertaken since the nogalose and bicyclic amino sugars are interacting with different bases and are oriented in opposite directions relative to the pyrimidine(3′–5′)purine intercalation site.

We observe that the nogalose sugar is nestled within the walls of the minor groove in the nogalamycin–d(A-G-C-A-T-G-C-T) complex in solution (Figure 8B). It has been known for some time that nonintercalating ligands such as netropsin bind to A·T-rich sites and are also nestled within the walls of a narrow minor groove in the crystalline state (Kopka et al., 1985) and in solution (Patel, 1982; Patel & Shapiro, 1985). Most interestingly, covalent adducts such as aminofluorene linked to the C8 position of guanosine and positioned opposite adenosine in a DNA oligomer duplex are accommodated by aligning the aminofluorene ring within the walls of the minor groove (Norman et al., 1989). Thus, our observation of van der Waals contacts between the nogalose sugar of nogalamycin and the base–sugar–phosphate backbone in the minor groove has precedent and may turn out to be an important general contribution to the stability of drug–DNA complexes. It should be noted that the nogalose sugar makes fewer intermolecular contacts with the minor groove in the complex in the crystalline state (Williams et al., 1990). This may reflect the different orientations observed for the nogalamycin–d(C-G-TsA-C-G) crystalline complex (**3**) and for the nogalamycin–d(A-G-C-A-T-G-C-T) solution complex (**4**).

The positively charged $N(CH_3)_2$ side chain on the bicyclic amino sugar is not hydrogen bonded to the phosphate backbone in the nogalamycin–DNA oligomer complexes in the crystalline (Liaw et al., 1989; Williams et al., 1990) and solution (Figure 10B) states. Rather, this charged group is positioned in the major groove in a plane between and parallel to the C3·G6 and G2·C7 base pairs. Previous studies have shown that the positively charged side chains of netropsin are positioned in the middle of the minor groove and do not hydrogen bond with the phosphate backbone (Kopka et al., 1985; Patel & Shapiro, 1985).

The structure of nogalamycin in the crystalline state (Arora, 1983) (Figure S5A) is compared with the structure of nogalamycin in its complex with the d(A-G-C-A-T-G-C-T) duplex in solution (Figure S5B). The overall structures are similar with the bicyclic amino and nogalose sugars on the same side of the aglycon plane. Both the bicyclic amino sugar and the nogalose sugars retain the chair conformation on complex formation in solution. The aglycon ring A retains the half-chair conformation with the carbomethoxy C10 group in the axial position on complex formation in solution. The principle difference between the crystalline structure of free nogalamycin and the solution structure of nogalamycin in its DNA complex is the small movement of the bicyclic amino and nogalose sugars toward each other in the complex. A similar observation was made in one of the crystallographic studies on nogalamycin complex formation with the d(C-G-TsA-C-G) duplex (Williams et al., 1990). This movement presumably results in improved van der Waals contacts between the nogalamycin sugars and the DNA grooves and helps to position the hydrogen-bond donor and acceptor groups for favorable pairing in the complex. This observation of an induced fit between antitumor agent and DNA has implications in drug design studies.

Future Studies. There are two areas open for further investigation: (1) We should be able to more accurately define the solution structure of the nogalamycin–d(A-G-C-A-T-G-C-T) complex by back-calculating the NOESY spectrum and through interactive refinement to minimize the differences with the experimental NOESY spectrum. Therefore, we believe it to be premature to list conformational parameters till these efforts are completed in the future. (2) We are intrigued by the alignment of nogalamycin sugar side chains in opposite directions between the crystallographic (**3**) and solution (**4**) studies. Clearly, the solution studies should be extended to sequences where the nogalamycin binding sites are separated by four base pairs and also where a direct comparison can be made between potential (C-A)·(T-G) and (C-G)·(C-G) intercalation sites. Thus, a study of nogalamycin binding to the self-complementary d(A-G-C-A-A-T-T-G-C-T) and d(A-G-C-G-A-T-C-G-C-T) duplexes should clarify some of the questions raised by the NMR and crystallographic results.

ACKNOWLEDGMENTS

We thank Dr. Jean-Louis Leroy for his contribution to the preparation of the nogalamycin–d(A-G-C-A-T-G-C-T) complex and the early NMR studies of the complex. We also thank Sophie Gueron, Ishver Radhakrishnan, and Michael Kouchakdjian for DNA synthesis and generation of the complex. The NMR spectrometers were purchased from funds donated by the Robert Woods Johnson, Jr., Trust and Matheson Trust toward setting up the NMR Center in the Basic Medical Sciences at Columbia University.

SUPPLEMENTARY MATERIAL AVAILABLE

Figures showing two-dimensional NOESY contour plots of the complex in H_2O and D_2O (Figure S1), expanded NOESY plots of the complex in D_2O recorded at mixing times of 100 and 50 ms (Figure S2), stereoviews of the structure of the complex with and without nogalamycin (Figure S3), stereoviews of the intercalation site without nogalamycin (Figure S4), and stereoviews of nogalamycin in the crystal and nogalamycin in the complex in solution (Figure S5) (6 pages). Ordering information is given on any current masthead page.

REFERENCES

Arora, S. K. (1983) *J. Am. Chem. Soc. 105*, 1328–1332.
Bhuyan, B. K., & Reusser, F. (1970) *Cancer Res. 30*, 984–989.
Borgias, B. A., & James, T. L. (1988) *J. Magn. Reson. 79*, 493.
Brooks, B. R., Bruccoleri, R. E., Olafson, B. D., States, D. J., Swaminathan, S., & Karplus, M. (1983) *J. Comput. Chem. 4*, 187–217.
Clore, G. M., & Gronenborn, A. M. (1984) *FEBS Lett. 172*, 219–225.
Clore, G. M., Nilges, M., Sukumaran, D. K., Brunger, A. T., Karplus, M., & Gronenborn, A. M. (1986) *EMBO J. 5*, 2729–2735.
Das, G. C., Dasgupta, S., & Dasgupta, N. N. (1974) *Biochim. Biophys. Acta 353*, 274–282.
Ennis, H. L. (1981) *Antimicrob. Agents Chemother. 19*, 657–665.
Fok, J., & Waring, M. J. (1972) *Mol. Pharmacol. 8*, 65–74.
Fox, K. R., & Waring, M. J. (1984) *Biochim. Biophys. Acta 802*, 162–168.
Fox, K. R., & Waring, M. J. (1986) *Biochemistry 25*, 4349–4356.
Fox, K. R., Brassett, C., & Waring, M. J. (1985) *Biochim. Biophys. Acta 840*, 383–392.
Gale, E. F., Cundliffe, E., Reynolds, P. E., Richmond, M. H., & Waring, M. J. (1981) *The Molecular Basis of Antibiotic Action*, Chapter 5, Wiley, London.
Gao, X., & Patel, D. J. (1989a) *Biochemistry 28*, 751–762.
Gao, X., & Patel, D. J. (1989b) *Q. Rev. Biophys. 22*, 93–138.
Gronenborn, A. M., & Clore, G. M. (1985) *Prog. Nucl. Magn. Reson. Spectrosc. 17*, 1–33.
Gronenborn, A. M., Clore, G. M., & Kimber, B. J. (1984) *Biochem. J. 221*, 723–736.
Hare, D. R., Wemmer, D. E., Chou, S. H., Drobny, G., & Reid, B. R. (1983) *J. Mol. Biol. 171*, 319–336.
Kersten, W., Kersten, H., & Szybalski, W. (1966) *Biochemistry 5*, 236–244.
Kopka, M. L., Yoon, C., Goodsell, D., Pjura, P., & Dickerson, R. E. (1985) *J. Mol. Biol. 183*, 553–563.
Lane, A. N. (1988) *J. Magn. Reson. 78*, 425.
Li, L. H., Kuentzel, S. L., Murch, L. L., Pschigoda, L. M., & Krueger, W. C. (1979) *Cancer Res. 39*, 4816–4822.
Liaw, Y. C., Gao, Y. G., Robinson, H., van der Marel, G. A., van Boom, J. H., & Wang, A. H. (1989) *Biochemistry 28*, 9913–9918.
Nerdal, W., Hare, D. R., & Reid, B. R. (1988) *J. Mol. Biol. 201*, 717–739.
Norman, D., Abuaf, P., Hingerty, B. E., Live, D., Grunberger, D., Broyde, S., & Patel, D. J. (1989) *Biochemistry 28*, 7462–7476.
Patel, D. J. (1982) *Proc. Natl. Acad. Sci. U.S.A. 79*, 6424–6428.
Patel, D. J., & Shapiro, L. (1985) *Biochimie 67*, 887–915.
Patel, D. J., Shapiro, L., & Hare, D. (1987) *Q. Rev. Biophys. 20*, 1–34.
Reid, B. R. (1987) *Q. Rev. Biophys. 20*, 1–34.
Ryckaert, J. P., Cicotti, G., & Berendson, H. J. C. (1977) *J. Comput. Phys. 23*, 327–337.
Searle, M. S., Hall, J. G., Denny, W. A., & Wakelin, L. P. (1988) *Biochemistry 27*, 4340–4349.
Sinha, R. K., Talapatra, P., Mitra, A., & Mazumder, S. (1977) *Biochim. Biophys. Acta 474*, 199–209.
Sobell, H. M., Jain, S. C., Sakore, T. D., & Nordman, C. E. (1971) *Nature, New Biol. 231*, 200–205.
Takusagawa, F., Dabrow, M., Neidle, S., & Berman, H. M. (1982) *Nature 296*, 466–469.
Van de Ven, F. J., & Hilbers, C. W. (1988) *Eur. J. Biochem. 178*, 1–38.
Verlet, L. (1976) *Phys. Rev. 159*, 98–105.
White, R. J., & Phillips, D. R. (1989) *Biochemistry 28*, 6259–6269.
Williams, D. H., Egli, M., Gao, Q., Bash, P., van der Marel, G. A., van Boom, J. H., Rich, A., & Fredrick, C. (1990) *Proc. Natl. Acad. Sci. U.S.A. 87*, 2225–2229.